

Symmetrically Threaded SQUIDS As Next Generation Kerr-cat Qubits

Bibek Bhandari,^{1,*} Irwin Huang,^{2,*} Ahmed Hajr,^{3,4} Kagan Yanik,² Bingcheng Qing,³ Ke Wang,³ David I Santiago,^{3,5} Justin Dressel,^{6,1} Irfan Siddiqi,^{3,5} and Andrew N Jordan^{7,6,1,2}

¹*Institute for Quantum Studies, Chapman University, Orange, CA 92866, USA*

²*Department of Physics and Astronomy, University of Rochester, Rochester, NY 14627, USA*

³*Quantum Nanoelectronics Laboratory, Department of Physics, University of California at Berkeley, Berkeley, CA 94720, USA*

⁴*Graduate Group in Applied Science and Technology, University of California at Berkeley, Berkeley, CA 94720, USA*

⁵*Computational Research Division, Lawrence Berkeley National Laboratory, Berkeley, Berkeley, CA 94720, USA*

⁶*Schmid College of Science and Technology, Chapman University, Orange, CA 92866, USA*

⁷*The Kennedy Chair in Physics, Chapman University, Orange, CA 92866, USA*

Kerr-cat qubits are bosonic qubits with autonomous protection against bit-flips. They have been studied widely using driven Superconducting Nonlinear Asymmetric Inductive eLement (SNAIL) oscillators. We theoretically investigate an alternate circuit for the Kerr-cat qubit, namely Symmetrically Threaded SQUIDS (STS). We perform the circuit analysis and derive the Gorini–Kossakowski–Sudarshan–Lindblad (GKLS) master equation for the Kerr-cat qubit attached to a thermal environment. We find that the lifetime time of the coherent states (T_α) of the Kerr-cat qubit is the same in both the STS and SNAIL circuits for weak Kerr nonlinearity. However, the STS Kerr-cat qubits have the additional benefit of being resistant against higher order photon dissipation effects, resulting in significantly longer T_α even with stronger Kerr nonlinearity on the order of 10 MHz. We also examine the effects of strong flux driving and asymmetric Josephson junctions on T_α . Unlike the SNAIL design, we find a dip in T_α of the STS Kerr-cat qubit for weak two-photon drive. However, we show that the dip can be mitigated by applying a suitable drive-dependent detuning. With the proposed design and considering a cat size of 10 photons, we predict T_α of the order of tens of milliseconds even in the presence of multi-photon heating and dephasing effects. The robustness of the STS Kerr-cat qubit makes it a promising component for fault-tolerant quantum processors.

I. INTRODUCTION

Creating artificial atoms using superconducting circuits is one of the most promising approaches to developing qubits for fault-tolerant quantum computation [1–5]. However, many of the superconducting qubit architectures suffer from low coherence time, limiting the gates and readout fidelities [2–9]. Here we investigate a noise-biased Kerr-cat qubit [4, 10–28] which has a long coherence time, observed close to a millisecond experimentally [13–15]. The static effective Hamiltonian describing a Kerr nonlinear oscillator subject to a two-photon drive (commonly referred to as a squeeze drive) consists of a double-well in the phase space representation. The tunneling between the two wells destructively interfere under certain conditions and give rise to noise-biased qubits which are strongly protected against bit-flip channels [29]. The static effective Hamiltonian, that governs the dynamics, obtained using a fast time-periodic driving, cannot be obtained by using just a static Hamiltonian. One can make a direct analogy to the case of a driven classical oscillator, namely the Kapitza pendulum, where the oscillator can be dynamically stabilized in an otherwise unstable point [30].

There are two main approaches to obtaining a cat qubit: 1) a quantum harmonic oscillator in the presence of engineered two photon dissipation [18, 31–38] and 2) two photon driving of a Kerr non-linear oscillator with a finite but small Kerr coefficient [4, 10, 11, 13–15]. The Kerr-cat qubit allows for simpler high fidelity non-demolition readout and faster gate operations. Kerr-cat qubits have been extensively studied, both theoretically [10, 14, 20, 21, 39–41] and experimentally [4, 13, 15], in a setup based on a SNAIL oscillator, which consists of a loop of multiple large Josephson junctions and a smaller Josephson junction, threaded by a DC magnetic flux. In this article, we present an alternate design based on symmetrically threaded SQUIDS (STS) as shown in Fig. 1(a). We will show that this design is resistant against multi-photon heating effects even with Kerr nonlinearity on the order of 10 MHz.

The Kerr-cat Hamiltonian is inevitably connected to an external environment leading to decoherence and dissipation. Heating effects due to single and multi-photon excitations in the qubit were predicted even at zero temperature in strongly driven systems [21]. However, one can exploit the degenerate spectrum of the Kerr-cat Hamiltonian to mitigate decoherence. In this article, we will discuss two different ways to increase the degeneracy in the STS Kerr-cat qubit spectrum: (1) increasing the two-photon drive strength studied in Refs. [13–15] and (2) obtaining a detuning nearly equal to a non-negative even integer multiple of the nonlinear Kerr coefficient

* These authors contributed equally; Correspondence should be addressed to: bbhandari@chapman.edu

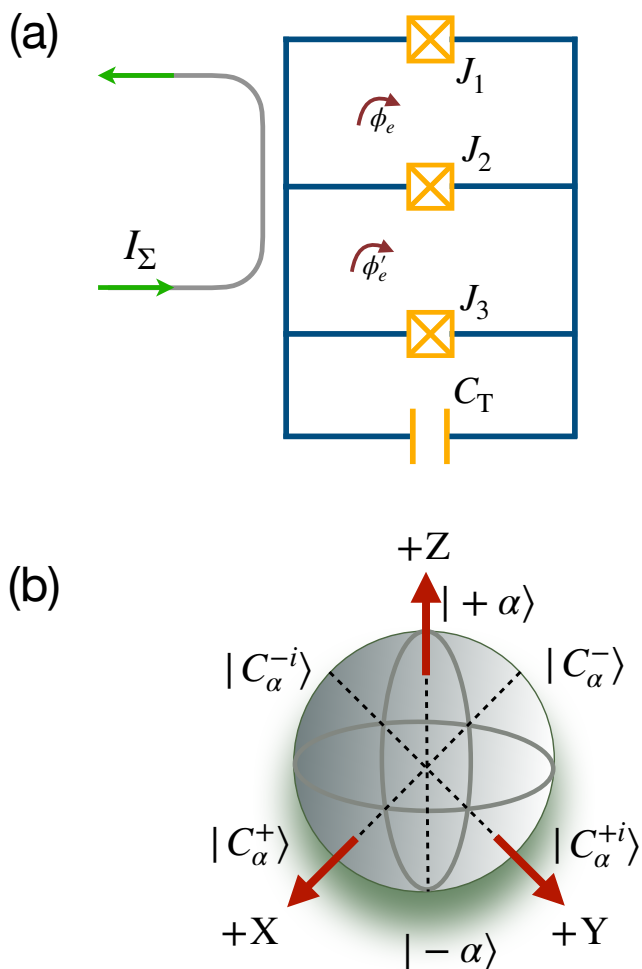


Figure 1. (a) STS design for Kerr-cat qubit. The junctions J_1 and J_3 compose the “SQUID branch” whereas the junction J_2 gives the “transmon branch”. The loop between J_1 and J_2 is threaded by an external flux ϕ_e whereas the loop between J_2 and J_3 is threaded by an external flux ϕ'_e . We consider $\phi'_e = \phi_e = -\pi/2 + \delta\phi \cos(\omega_d t)$. C_T is the shunt capacitor associated with the transmon branch. (b) Bloch sphere representation of the Kerr-cat qubit states.

studied in Refs. [13–15]. We find that the number of degeneracies in the spectrum increases faster when both the two-photon drive strength and detuning are increased simultaneously, leading to an enhancement in the lifetime of the coherent states (T_α) of the qubit [14].

There are two major differences between the flux-driven STS design and the charge-driven SNAIL design [4, 13]: (1) The presence of an extra term that we interpret as a drive-dependent detuning term in the static effective Hamiltonian [42] which is absent in the SNAIL case. (2) In the STS design, even and odd harmonics appear at different orders of zero point spread of the phase operator depending on the symmetric and asymmetric part of the SQUID junctions, respectively. We find that the leading order multi-photon heating effects, which are

observed to significantly reduce T_α in the SNAIL design for large Kerr coefficient, are proportional to the asymmetry of SQUID junctions and can be mitigated by making the junctions as symmetric as possible. This leads to robust T_α in the STS Kerr-cat design even in the high Kerr coefficient limit.

We start with a model for the Kerr-cat Hamiltonian in the next section. In Sec. II A, we present an alternate circuit based on driven STS for the Kerr-cat qubit and calculate its static effective Hamiltonian. In Sec. III, we investigate the static effective master equation up to leading order in system-environment coupling and fourth order in zero point phase spread taking into account the asymmetry of the Josephson junction. Using the derived master equation, in Sec. IV we study T_α of the STS Kerr-cat qubit as a function of two-photon drive strength and detuning. We also compare the robustness of the proposed design with a single SQUID and SNAIL designs in Sec. IV B. In the absence of detuning, the first two Fock states become the cat states in the presence of the two-photon drive. However, since this is not the case for detuned qubits, we investigate the qubit initialization process in detuned Kerr-cat qubits in Sec. IV C. Finally, in Sec. V we draw our conclusions.

II. KERR-CAT HAMILTONIAN

Let us consider a nonlinear quantum oscillator described by the Hamiltonian[10, 11]

$$\hat{H}_{KC} = \Delta \hat{a}^\dagger \hat{a} + \epsilon_2 (\hat{a}^{\dagger 2} + \hat{a}^2) - K \hat{a}^{\dagger 2} \hat{a}^2, \quad (1)$$

where Δ is the detuning term, K is the Kerr nonlinearity, and ϵ_2 is the two-photon drive strength that excites and annihilates photons in pairs. The two-photon drive has been traditionally realized in SNAIL oscillators by applying a charge drive at twice the oscillator frequency[4, 13–15]. For $\Delta = 0$, the coherent states $|\pm\alpha\rangle$ with $\alpha = \sqrt{\epsilon_2/K}$ are the eigenstates of the above Hamiltonian. The cat states are the even/odd parity states formed by the superposition of coherent states

$$|C_\alpha^\pm\rangle = \frac{1}{\sqrt{2}} \frac{1}{\sqrt{1 \pm e^{-2\alpha^2}}} (|\alpha\rangle \pm |-\alpha\rangle). \quad (2)$$

In the effective low dimensional subspace, the eigenstates of \mathbf{Z} , $\mathbf{Z}|\pm Z\rangle = \pm|\pm Z\rangle$ are shown as bases in the Bloch sphere representation (see Fig. 1(b)) where

$$|\pm Z\rangle = \frac{1}{\sqrt{2}} (|C_\alpha^+\rangle \pm |C_\alpha^-\rangle) \approx |\pm\alpha\rangle. \quad (3)$$

The other Pauli operators can be defined accordingly [43].

A. STS circuit analysis and Hamiltonian

To realize the Hamiltonian in Eq. (1), we consider an alternative circuit for Kerr-cat qubit based on the STS.

The circuit design is shown in Fig. 1(a). For the sake of simplicity, we will consider only one STS circuit with single junctions and later discuss the implications of having multiple junctions in the transmon branch and multiple STS in series. An external flux $\phi_e(\phi'_e)$, in units of flux quantum $h/2e$, is threaded through the SQUID loop formed by Josephson junctions J_2 and $J_1(J_3)$. A capacitor C_T is connected in parallel to the junction arrays. The Hamiltonian for the circuit in the lab frame can be written as [44]

$$\begin{aligned} \hat{H}_{\text{lab}} = & 4E_C \hat{n}^2 - E_{J1} \cos\left(\hat{\varphi} + \frac{2}{3}\phi_e + \frac{1}{3}\phi'_e\right) \\ & - E_{J2} \cos\left(\hat{\varphi} + \frac{1}{3}\phi_\Delta\right) - E_{J3} \cos\left(\hat{\varphi} - \frac{1}{3}\phi_e - \frac{2}{3}\phi'_e\right), \end{aligned} \quad (4)$$

where we considered equal junction capacitances. E_{Ji} , $i = 1, 2, 3$, gives the Josephson energy of the Josephson junction J_i and E_C is the effective capacitive energy.

When the flux is asymmetrically threaded between the two loops, it was shown that one can implement efficient 4-wave mixing processes in the ATS (Asymmetrically Threaded SQUID) [32]. However, since we are interested in doing efficient 3-wave mixing to generate the two-photon drive, we instead thread the flux symmetrically using $\phi_\Delta = \phi'_e - \phi_e = 0$. Eq. (4) reduces to

$$\begin{aligned} \hat{H}_{\text{lab}} = & 4E_C \hat{n}^2 - E_{J2} \cos \hat{\varphi} - 2E_{J\Sigma} \cos \phi_e \cos \hat{\varphi} \\ & + 2E_{J\Delta} \sin \phi_e \sin \hat{\varphi}, \end{aligned} \quad (5)$$

where we defined $E_{J\Sigma} = (E_{J1} + E_{J3})/2$ and $E_{J\Delta} = (E_{J1} - E_{J3})/2$. For the sake of simplicity, we consider $E_{J\Delta} = 0$ in this section. Note that the effective capacitance (including the junction capacitance as well as the external capacitor C_T) along with the junction J_2 will act as a transmon providing the necessary bound states and the Kerr nonlinearity for the oscillator. To generate a large two-photon drive, we symmetrically DC bias the SQUID around $-\pi/2$, then apply an AC modulation tone according to $\phi_e = \phi'_e = -\pi/2 + \delta\phi \cos(\omega_d t)$. The DC bias point is chosen to create the highest first-order sensitivity on the modulation depth $\delta\phi$ while removing the parasitic even harmonics of the drive (see Appendix A).

Expanding the Hamiltonian in Eq. (5) to fourth order in $\hat{\varphi} = \varphi_{\text{zps}}(\hat{a}^\dagger + \hat{a})$ with $\varphi_{\text{zps}} = (2E_C/E_J)^{1/4}$ being the zero point phase spread, we obtain

$$\begin{aligned} \hat{H}_{\text{lab}} = & \epsilon_c \hat{a}^\dagger \hat{a} - K \hat{a}^{\dagger 2} \hat{a}^2 - 2E_{J\Sigma} \sin(\delta\phi \cos(\omega_d t)) \\ & \sum_{n=1,2} \frac{(-1)^n}{(2n)!} [\varphi_{\text{zps}}(\hat{a} + \hat{a}^\dagger)]^{2n}, \end{aligned} \quad (6)$$

where $\epsilon_c = \sqrt{8E_C E_{J2}}$ and $K = E_C/2$. In order to obtain the Kerr-cat Hamiltonian of Eq. (1), we look for the static effective representation of \hat{H}_{lab} under the condition $\hbar\omega_d \approx 2\epsilon_c$.

Going to the rotating frame at frequency $\omega_d/2$ following the transformation $\hat{a} \rightarrow \hat{a}e^{-i\omega_d t/2}$ and using

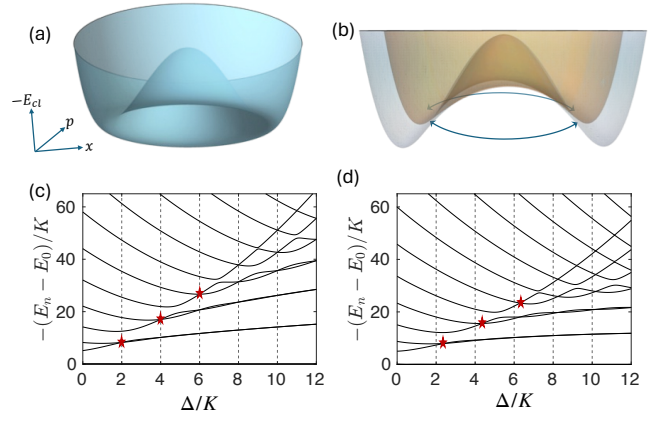


Figure 2. Classical phase space surface of the total effective energy of the Kerr-cat Hamiltonian in Eq. (7) for $\Delta = 4K$, (a) $\epsilon_2 = \Lambda = 0$, and (b) $\epsilon_2 = 0.3K$, $\Lambda = 0$ (yellow plot) and $\Lambda = 0.2K$ (grey plot). Energy spectrum of Eq. (7) as a function of Δ for $\epsilon_2 = 2K$ and (c) $\Lambda = 0$ and (d) $\Lambda = 0.12K$. Red stars denote the first degeneracies of the first three excited state pairs with opposite parity.

the generalized Schrieffer-Wolff transformation generated by $\hat{S}(t) = \mathcal{O}(\varphi_{\text{zps}})$ (see Appendix A for details), the effective Hamiltonian for the STS is given by $\hat{\mathcal{H}}_S = e^{\hat{S}/i\hbar} \hat{H}_{\text{lab}}(t) e^{-i\hat{S}/i\hbar} - i\hbar e^{\hat{S}/i\hbar} \partial_t e^{\hat{S}/i\hbar}$. Up to $\mathcal{O}(\varphi_{\text{zps}}^4)$, the static effective Hamiltonian is given by

$$\hat{\mathcal{H}}_S = \Delta \hat{a}^\dagger \hat{a} + \epsilon_2 (\hat{a}^{\dagger 2} + \hat{a}^2) - K \hat{a}^{\dagger 2} \hat{a}^2 + \Lambda (\hat{a}^\dagger \hat{a}^3 + \hat{a}^{\dagger 3} \hat{a}), \quad (7)$$

where for STS with single junctions of energy $E_{J1} = E_{J2} = E_{J3} = E_J$ and up to first order in the modulation depth $\delta\phi$,

$$\epsilon_2 = \delta\phi/2 \left(\sqrt{2E_C E_J} - E_C \right) = \delta\phi/4 (\epsilon_c - 2E_C), \quad (8)$$

$\Delta = \epsilon_c - \hbar\omega_d/2 - 2K - \delta\phi^2 \epsilon_c^2 / 8\hbar\omega_d$, $K = E_C/2$ and $\Lambda = -\delta\phi E_C/3$. Note that the two-photon drive strength ϵ_2 is linear in the modulation depth, the oscillator frequency, and the charging energy E_C . Compared with the usual Kerr-cat Hamiltonian studied in Refs. [4, 10] and given in Eq. (1), the static effective Hamiltonian in Eq. (7) for STS has an extra term proportional to Λ . We will analyze the effect of this term on the qubit states and the lifetime of the qubit in the next section.

In Fig. 2(a), we show the total effective classical energy (E_{cl}) of a non-linear oscillator ($\epsilon_2 = 0$) in the phase space. We observe a circularly symmetric energy well in the position (x) and momentum (p) space. The interwell tunneling can only take place through the barrier in the middle. However, in the case of Kerr-cat qubit (see Fig. 2(b)), a classically forbidden region develops in between the double well. Further, two saddle points connect the two wells. The tunneling through these saddle points can destructively interfere, giving rise to robust qubits. In Ref. [14], it was shown that the destructive interference happens when the detuning is an integer multiple

of the Kerr coefficient, $\Delta = 2mK$, m is a non-negative integer.

In Fig. 2(c), we plot the energy spectra of the Kerr-cat qubit as a function of detuning for $\Lambda = 0$ which is equivalent to a SNAIL Kerr-cat Hamiltonian [21]. For $\Delta/K = 2m$, we observe $m + 1$ degeneracy points; note that the ground state energies of a Kerr-cat Hamiltonian, which are subtracted from the eigenenergies, are always degenerate. The main difference between our analysis based on STS and Ref. [10] can be seen in Fig. 2(d) where we plot the energy spectra for $\Lambda = 0.12K$, recalling that, Λ is absent in the SNAIL Kerr-cat Hamiltonian. Although the degeneracy points are independent of the values of ϵ_2 in SNAIL Kerr-cats, we find that with STS they get shifted from $\Delta/K = 2m$ for finite values of Λ . Since, Λ and ϵ_2 both depend on the modulation depth $\delta\phi$, the shift in degeneracy varies as a function of ϵ_2 . We can thus apply an external drive-dependent detuning to cancel the shift in degeneracy points.

The lab Hamiltonian in Eq. (6) consists of a transmon type contribution (the first two terms) and a SQUID type contribution (the last two terms). The transmon part is obtained from the middle branch of the STS, whereas the SQUID contribution is obtained from the outer branches. From now on, we will call the middle branch with Josephson junction J_2 as the ‘‘transmon branch’’ whereas the other branches will be referred to as the ‘‘SQUID branch’’. In order to dilute the Kerr (necessary to mitigate multi-photon heating effects), we will consider multiple STS connected in series. Let us consider M number of STS with a single junction in the SQUID branch. In that case, if \tilde{N} number of junctions are used in series in the transmon branch of each STS (each with Josephson energy $E'_{J2} = NE_{J2}$, where $N = M\tilde{N}$), the Kerr coefficient gets diluted to $K \rightarrow K/N^2$ (see Appendix A1 for details). Since the Kerr coefficient and the two-photon drive strength compete to stabilize the cat states, one can enhance the effect of pumping without increasing the modulation depth by just diluting the Kerr coefficient.

III. STATIC EFFECTIVE GKLS MASTER EQUATION

In this section, we consider an open quantum system to study the lifetime of the coherent states of the STS Kerr-cat qubit in the presence of an external environment. The environment is considered to be a macroscopic system at thermal equilibrium with temperature T composed of a bath of linear oscillators with continuous modes. The Hamiltonian for the bath is given by

$$\hat{H}_B = \sum_j \hbar\omega_j \hat{b}_j^\dagger \hat{b}_j, \quad (9)$$

where \hat{b}_j and \hat{b}_j^\dagger are, respectively, the annihilation and creation operators of an excitation of energy $\hbar\omega_j$ in the

environment. The system environment coupling Hamiltonian in the rotating frame takes the following form

$$\hat{H}_{SB}(t) = i \left(\hat{a} e^{-i\omega_d t/2} - \hat{a}^\dagger e^{i\omega_d t/2} \right) \hat{B}(t), \quad (10)$$

where $\hat{B}(t) = \sum_j i h_j \left(\hat{b}_j e^{-i\omega_j t} - \hat{b}_j^\dagger e^{i\omega_j t} \right)$ and h_j gives the coupling strength.

For a system which is weakly coupled to a thermal environment with fast dynamics such that any excitation in the environment induced by the system is quickly carried away, the dynamics of the system is given by the GKLS master equation,

$$\frac{d\hat{\rho}_S}{dt} = -\frac{i}{\hbar} \left[\hat{\mathcal{H}}_S, \hat{\rho}_S \right] + \sum_l \gamma_l \mathcal{D}[\hat{O}_l] \hat{\rho}_S, \quad (11)$$

where $\mathcal{D}[\hat{O}_l] \hat{\rho}_S = \hat{O}_l \hat{\rho}_S \hat{O}_l^\dagger - \left(\hat{O}_l^\dagger \hat{O}_l \hat{\rho}_S + \hat{\rho}_S \hat{O}_l^\dagger \hat{O}_l \right) / 2$ for the jump operator \hat{O}_l and γ_l is the corresponding transition rate. The first term in the right hand side of Eq. (11) gives the unitary dynamics due to the system Hamiltonian and the second term gives the dissipation introduced by the environment.

In the frame introduced by the Schrieffer-Wolff transformation generated by $\hat{S}(t)$, although the system Hamiltonian is static, the transformed system environment Hamiltonian would not necessarily be static. The transformed system environment coupling up to $\mathcal{O}(\varphi_{zps}^2)$ is given by (see Appendix B for details)

$$\hat{\mathcal{H}}_{SB}^{(2)}(t) = \hat{H}_{SB}(t) + \frac{iG_{2,S}}{\hbar\omega_d} \left\{ 3(-\hat{a}^\dagger e^{i3\omega_d t/2} + \hat{a} e^{-i3\omega_d t/2}) + 2(-\hat{a} e^{i\omega_d t/2} + \hat{a}^\dagger e^{-i\omega_d t/2}) \right\} \hat{B}(t), \quad (12)$$

where $G_{2,S} = \delta\varphi E_{J\Sigma} \varphi_{zps}^2 / 2$. The corresponding GKLS master equation is given by

$$\begin{aligned} \frac{\partial \hat{\rho}_S(t)}{\partial t} &= \left\{ \gamma(\omega_d/2) \mathcal{D}[\hat{a}^\dagger] + \Upsilon(\omega_d/2) \mathcal{D}[\hat{a}] \right\} \hat{\rho}_S(t) \\ &+ \left(\frac{3G_{2,S}}{\hbar\omega_d} \right)^2 \left\{ \gamma(3\omega_d/2) \mathcal{D}[\hat{a}^\dagger] + \Upsilon(3\omega_d/2) \mathcal{D}[\hat{a}] \right\} \hat{\rho}_S(t), \end{aligned} \quad (13)$$

where $\frac{\partial \hat{\rho}_S(t)}{\partial t} = \frac{\partial \hat{\rho}_S(t)}{\partial t} - \frac{1}{i\hbar} [\hat{\mathcal{H}}_S, \hat{\rho}_S(t)]$ and $\hat{a} = \hat{a} + \frac{2G_{2,S}}{\hbar\omega_d} \hat{a}^\dagger$. $\gamma(\omega) = \hbar^{-1} \kappa(\omega) n(\omega)$ and $\Upsilon(\omega) = \hbar^{-1} \kappa(\omega) (1 + n(\omega))$ are the incoming (from the environment to the qubit) and the outgoing (from the qubit to the environment) transition rates, respectively. $\kappa(\omega) = 2\pi \hbar^{-1} \sum_j |h_j|^2 \delta(\omega - \omega_j)$ is the spectral density and $n(\omega) = [e^{\hbar\omega/k_B T} - 1]^{-1}$ is the Bose-Einstein distribution function of the environment. The system-environment coupling and the master equation up to $\mathcal{O}(\varphi_{zps}^4)$ are calculated in Appendix B.

The first line on the right hand side of Eq. (13) gives the master equation under the rotating wave approximation (RWA) for $\hat{a} \rightarrow \hat{a}$. Unlike the SNAIL case, we

observe that up to the leading order beyond RWA the master equation contains only single-photon effects. For symmetric SQUID junctions, we do not observe two-photon heating and cooling effects, even at higher orders of φ_{zps} . The next order terms include three-photon effects at $\mathcal{O}(\varphi_{zps}^4)$ (see Appendix B). However, the asymmetry in SQUID junctions can result in two-photon heating and cooling effects, which will be discussed more in detail in the next section. Note that we undergo several approximations to derive the GKLS master equation: 1) Born approximation which demands weak system-environment coupling, i.e. $V_k \ll \epsilon_c \varphi_{zps}^2$, 2) Fast bath dynamics compared to the system relaxation time (Markov approximation), and 3) weak zero point phase spread (φ_{zps}) and modulation depth ($\delta\phi$). Further, the derived master equation in this section only includes the linear tunneling Hamiltonian and does not account for dephasing. We will later add a term proportional to the number operator in the Lindbladian to study the effect of dephasing (see Sec. IV A).

With symmetric SQUIDs, we only get terms proportional to even powers of the φ_{zps} in both the static effective Hamiltonian as well as the master equation. However, when the asymmetry in the SQUID junctions are taken into account, all order in φ_{zps} contribute. This introduces extra terms in the static effective Hamiltonian and two-photon heating and cooling effects in the master equation, which are absent in the symmetric case (see the $\mathcal{O}(\varphi_{zps}^3)$ master equation in Appendix B). We find that the multi-photon dissipative effects due to 5% asymmetry in the SQUID junction result in a negligible reduction of T_α for $K < 10$ MHz. Further, two-photon drive strength (ϵ_2/K) depends on both the Kerr coefficient and the modulation depth ($\delta\phi$). In the high Kerr coefficient limit, stronger modulation is required to obtain large enough two-photon drive strength; the first order approximation, $\sin(\delta\phi \cos(\omega_d t)) \approx \delta\phi \cos(\omega_d t)$, breaks down and one has to consider higher order terms in the modulation depth, $\delta\phi$. We do the calculation for stronger modulation depth in Appendix B 3. The result is a longer first plateau in T_α plots which will be discussed in detail in the next section.

IV. RESULTS

The staircase type pattern as a function of the two-photon drive strength is the most remarkable feature of the T_α plot in Fig. (3). This pattern has been analyzed and explained in detail in Refs. [13, 21]. For $\epsilon_2/K \rightarrow 0$, T_α of the Kerr-cat qubit is effectively given by the lifetime of the coherent superposition, $(|0\rangle \pm |1\rangle)/\sqrt{2}$, where $|0\rangle$ ($|1\rangle$) are the ground (first excited state) of the Kerr nonlinear oscillator. The Kerr non-linearity along with the two-photon drive creates a double-well potential in the phase space (see Fig. 2 (a) and (b)). The exponential growth of T_α with increasing two-photon drive strength (ϵ_2/K) can be attributed to the inclusion of energy levels inside the double-well meta-potential. The

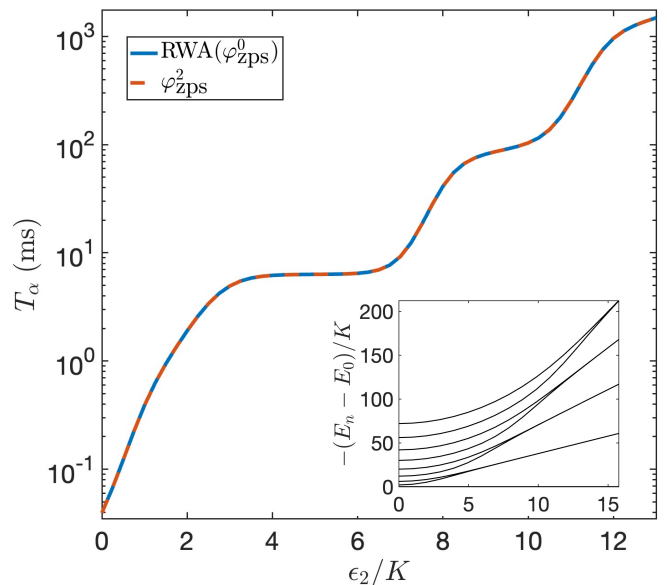


Figure 3. T_α of the Kerr-cat qubit as a function of the two-photon drive strength ϵ_2/K for 10 STS connected in series with a single junction in each branch setting the Kerr non-linearity to $K/h = 1.25$ MHz. The RWA calculation which takes the system environment coupling up to order $\varphi_{zps}^{(0)}$ and keeps only single photon processes in the master equation is given by the solid blue line. The dashed orange curve gives the leading order beyond RWA $\mathcal{O}(\varphi_{zps}^{(2)})$ calculation and keeps multiphoton processes in the master equation. In the inset, we plot the energy spectra of the Kerr-cat qubit as a function of the two-photon drive strength ϵ_2/K .

number of bound states inside the double-well potential is approximately given by $\mathcal{N} = \epsilon_2/\pi K$ [13] with a new pair of excited states entering the potential well every time \mathcal{N} takes an integer value. As shown in the inset of Fig. (3), the splitting between the energy levels entering the potential well becomes smaller with increasing ϵ_2 . Furthermore, the quantum tunneling between the two levels inside the double-well gets suppressed with decreasing splitting and becomes maximally protected from tunneling for degenerate states. This leads to an exponential growth in life time as a function of the two-photon drive strength. However, in order to explain the plateau in Fig. (3), we would have to consider the effect of the environment. T_α increases as a function of decreasing detuning until the rate of dissipation (γ) to the environment overcomes it. The tunneling between the two nearly degenerate states and the dissipation to the environment compete with each other resulting in lifetime saturation at $T_\alpha = (\gamma n_{th})^{-1}$ when only single photon heating and cooling effects are considered. As long as one takes the RWA, the plateau occurs at the same lifetime (T_α). However, non RWA terms can result in the lowering of the lifetime plateau. The second exponential growth starts when the next set of excited states fall into the meta-potential and the splitting between them decreases as a

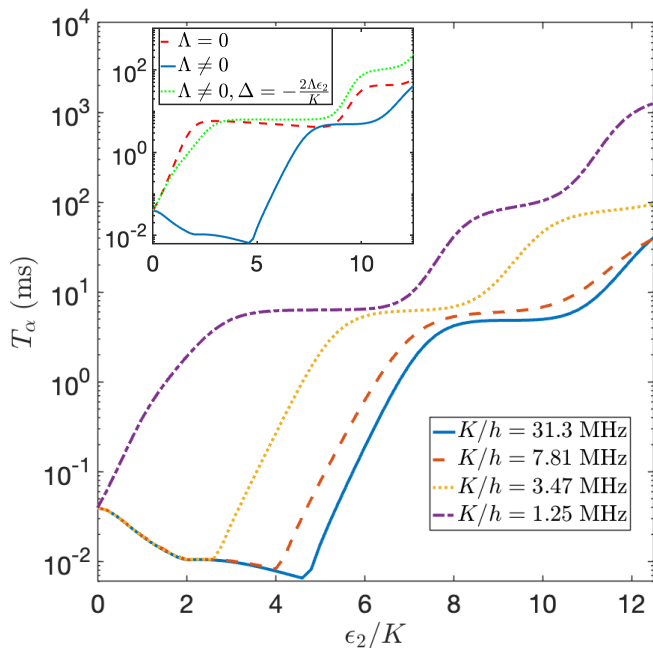


Figure 4. T_α of the Kerr-cat qubit as a function of the two-photon drive strength ϵ_2/K for different values of Kerr non-linearity. In order to obtain the mentioned Kerr-nonlinearity, we took $M = 2, N = 2$ (solid blue curve), $M = 2, N = 4$ (dashed orange curve) and $M = 3, N = 6$ (dotted yellow curve) and $M = 10, N = 10$ (dot-dashed purple curve). In the inset, we show how the initial dip in the lifetime observed for $K/h = 31.3$ MHz can be actively cancelled by introducing a drive-dependent detuning.

function of the two-photon drive strength. Unlike the SNAIL qubit, we observe that the STS qubit is well approximated in the RWA regime [21]. This is because the STS master equation does not contain terms on the order of φ_{zps}^1 . Therefore, the next largest contribution is on the order of φ_{zps}^2 , which is much smaller than the terms that survive RWA. Hence, the multi-photon heating and cooling effect is largely suppressed in the STS Kerr-cat qubits even when asymmetry between the Josephson energies are properly accounted. For the simulation parameters, we take the coupling to the external environment, $\gamma(\omega_d/2)/h = \gamma(3\omega_d/2)/h = 8$ kHz. For the temperature of the environment, we choose $T_{\omega_d/2} = T_{3\omega_d/2} = 50$ mK. Moreover, the Josephson energy for the transmon and SQUID junctions are considered to be of similar magnitude. The Josephson and capacitive energy are given by $E_J/h = 80$ GHz and $E_C/h = 250$ MHz respectively, and consequently the Kerr coefficient for a single junction is $K/h = 125$ MHz. Further, the drive frequency is given by $\omega_d = 24\pi$ GHz. Unless mentioned otherwise, we consider the detuning, $\Delta = 0$. The parameters were chosen to match the experimental conditions [13, 15].

The main difference between the usual Kerr-cat Hamiltonian [10] and the static effective Hamiltonian in Eq. (7) is the presence of the last term, $\Lambda(\hat{a}^\dagger \hat{a}^3 + \hat{a}^{\dagger 3} \hat{a})$. The most

dominant contribution to Λ is $\mathcal{O}(\varphi_{\text{zps}}^4)$, hence it is significantly smaller for $E_C \ll E_{J2}$. However, for larger values of Kerr coefficient which is also $\mathcal{O}(\varphi_{\text{zps}}^4)$, Λ becomes significant. The extra term proportional to Λ is responsible for the observed dip in T_α for $K/h = 31.3$ MHz (solid blue curve in Fig. 4 where we consider only two junctions in the transmon branch). The average effect of this term is to introduce an additional detuning proportional to $\Lambda(\hat{a}^{\dagger 2} + \hat{a}^2)$. This additional detuning takes the Kerr-cat qubit away from the sweet spot where the detuning is an even multiple of the Kerr coefficient. Apart from the dip in the T_α , we also observe a decrease in the plateau height for $K/h = 31.3$ MHz which results from the non RWA terms in the master equation. Increasing the Kerr coefficient, one eventually increases the effect of higher order in φ_{zps} terms. The above behavior motivates us to consider the case where the Kerr coefficient can be significantly reduced hence mitigating the unwanted contribution from the extra term in the STS Hamiltonian as well as non-RWA multi-photon effects. One possible way, as suggested in the Sec. (II A) is to consider the case with multiple junctions instead of a single junction in the transmon branch. This leads to the dilution of Kerr coefficient by $K \rightarrow K/(M\tilde{N})^2$, where \tilde{N} is defined through $N = M\tilde{N}$. M is the number of STS in series and \tilde{N} is the number of junctions in the transmon branch of each STS (see Appendix A 1 for details). In Fig. 4, the smaller Kerr coefficients are obtained by considering different number of STS in series, namely $M = 2$ (dashed orange curve), $M = 3$ (dotted yellow curve) and $M = 10$ (dot-dashed purple curve). We find that increasing the number of STS in series decreases the value of the two-photon drive strength required for initiating the exponential growth of life time ($\epsilon_2/K \approx 4.5$ for $M = 2$ whereas $\epsilon_2/K \approx 2.5$ for $M = 3$). Further, with sufficient number of STS which ensures sufficient reduction in the Kerr coefficient (from $K/h = 31.3$ MHz for $M = N = 2$ to $K/h = 1.25$ MHz for $M = N = 10$), one can get rid of the dip in the T_α as well as the lowering of the plateau altogether. We further observe that although the T_α curve still has a dip for $K/h = 3.47$ MHz (dotted yellow curve), the plateau height has been restored to the level of the purple curve. This implies that the multi-photon dissipative effects decay faster as a function of decreasing Kerr coefficient compared to the additional detuning introduced by Λ .

We find that one has to increase the number of STS to almost 10 to get rid of the dip in the T_α due to the extra term in the STS Kerr-cat Hamiltonian. Experimentally, it will be challenging to have so many STS in series. Instead of adding STS, one can think of actively cancelling the effect of the extra term. In the inset of Fig. 4, we propose a strategy to cancel the dip in the T_α for $M = 2, N = 2$ case (solid blue curve in the main plot). The idea is to add an extra drive dependent detuning in the circuit which is opposite in sign compared to the extra term proportional to Λ which results in a STS Kerr-cat Hamiltonian of Eq. (7) with $\Delta = -2\Lambda\epsilon_2/K$

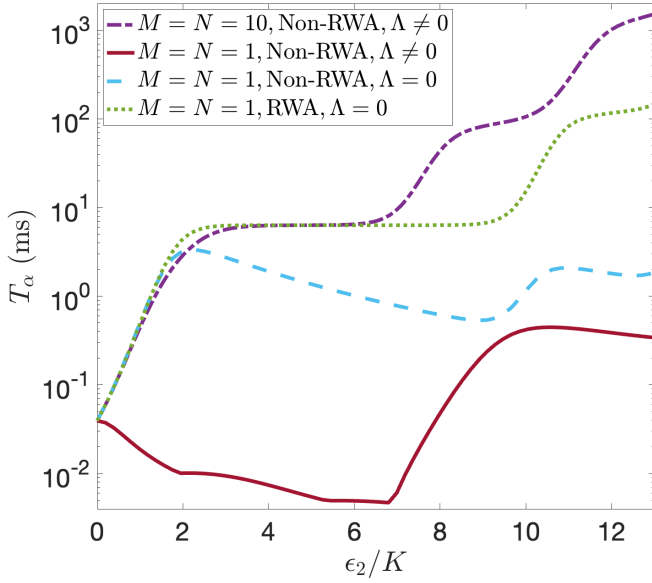


Figure 5. T_α of the Kerr-cat qubit as a function of the two-photon drive strength ϵ_2/K under strong modulation depth. The purple dot-dashed curve is obtained for 10 STS connected in series with $\tilde{N} = 1$ number of junction in the transmon branch which results in a small Kerr coefficient, $K/h = 1.25$ MHz. For the rest of the curves, we consider $M = N = 1$. The solid red curve is obtained by going up to $\mathcal{O}(\delta\phi^3)$ in the modulation depth and includes both non-RWA effects and effects due to finite Λ up to $\mathcal{O}(\varphi_{zps}^4)$. For $\Lambda = 0$, we have the dotted green and dashed blue curves obtained with RWA and taking into account the non RWA effects, respectively. We set $E_J/h = 200$ GHz for this particular lifetime calculation only.

since $\Lambda (\hat{a}^\dagger \hat{a}^3 + \hat{a}^{\dagger 3} \hat{a}) \approx (2\Lambda\epsilon_2/K) \hat{a}^\dagger \hat{a}$. We find that with this additional drive dependent detuning, the T_α plot for $M = 2, N = 2$ (green dotted curve) has no initial dip and almost overlaps the plot done for $\Lambda = 0$ (dashed red curve), recovering the staircase type pattern observed for low Kerr coefficient.

In order to further understand the effect of large Kerr coefficient on the the lifetime of the coherent states, we plot T_α for $N = 1$, i.e. $K/h = 125$ MHz under different considerations in Fig. 5. We set $E_J/h = 200$ GHz for the T_α calculation in Fig. 5. This allows us to investigate the strong modulation depth regime (up to third order in $\delta\phi$) with $M = N = 1$. The solid red curve gives the T_α plot taking into account multi-photon effects, finite Λ and stronger modulation depth. The solid blue curve in Fig. 4 was obtained for the same set of parameters but taking only leading order term in the modulation depth $\delta\phi$. The difference is a longer first plateau when stronger modulation depth is considered (compare the plateau for dashed blue curve in Fig. 5 and the green dotted curve in the inset of Fig. 4). We find that once we set $\Lambda = 0$, the dip in T_α vanishes (dashed blue curve). However, T_α decreases as a function of the two-photon drive strength for $\epsilon_2/K \gtrsim 2$ and finally aligns with the solid red curve

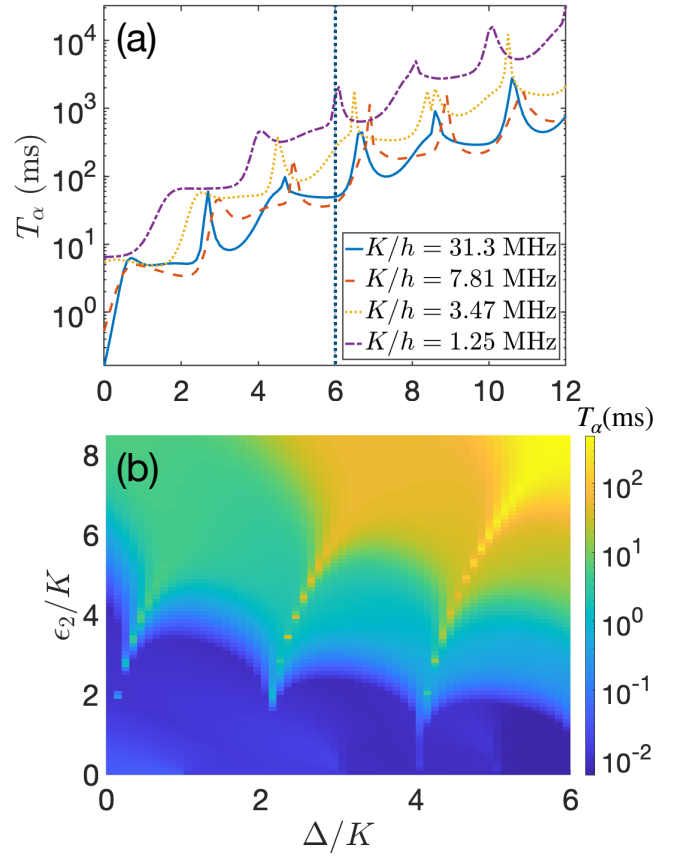


Figure 6. T_α of the Kerr-cat qubit (a) as a function of Δ/K for $\epsilon_2/K = 6$ and for different values of Kerr coefficient (same as Fig. 4) and (b) as a function of both ϵ_2/K and Δ/K for $M = 2, N = 4$ ($K/h = 7.81$ MHz).

before increasing again. Next, we consider only the RWA terms neglecting all the multiphoton effects taking $\Lambda = 0$ and find that the staircase type behavior of T_α has been restored (dotted green curve). The first plateau aligns with the case of small Kerr coefficient obtained with $M = N = 10$ (dot dashed purple curve). Note that even when the multi-photon heating and cooling effects as well as finite detuning due to Λ are neglected, T_α plateau gets longer for higher Kerr coefficient demanding stronger two-photon drive for a similar enhancement in T_α .

A. Detuning and dephasing dependence of T_α

For small Kerr coefficient, we have observed that T_α of the STS Kerr-cat qubit depends only on the two-photon drive strength, i.e. the ratio ϵ_2/K . We further observed that as the two-photon drive strength increases, the number of bound states inside the double-well and the number of degenerate states increases leading to enhancement of T_α . However, so far we have not looked into the effect of detuning (Δ) on T_α of the Kerr-cat qubit. In Fig. 6(a), we study the lifetime as a function of detuning. As men-

tioned in Sec. II A, the inter-well tunneling through the saddle points destructively interfere giving $m + 1$ degeneracies for $\Delta = 2mK$. These degeneracies lead to sharp spike in the T_α plots for even integer values of Δ/K as shown in Fig. 6(a) [14]. Note that the spikes are shifted a bit from the even integer values of Δ/K for larger values of Kerr coefficient (follow the black dashed line) where the extra detuning introduced by Λ is stronger. This shift results from the shift in degeneracy points in the energy spectra for finite values of Λ (see Fig. 2(d)). In Fig. 6(b), we plot T_α as a function of both the detuning Δ/K and the two-photon drive strength ϵ_2 . In Ref. [14], it was shown that the number of excited states entering the double-well increases faster when both ϵ_2/K and Δ/K are increased instead of just the two-photon drive strength. We observe similar features in Fig. 6 (b). One can analyze the lifetime plot fixing Δ/K to 1 and 6 and observe that lifetime increases significantly as function of ϵ_2/K for $\Delta/K = 6$. Also note the sharp spikes in lifetime around even integer values of Δ/K as observed in Fig. 6(a).

In order to understand the effect of dephasing on T_α , we add an extra term to the master equation, $L_\phi = \gamma_\phi \hat{a}^\dagger \hat{a}$, where γ_ϕ determines the dephasing strength. In Fig. 7, we plot the lifetime as a function of the two-photon drive strength for different values of the dephasing strength. We consider 10 STS connected in series with a single junction in each branch. The dot-dashed purple curve done for no dephasing matches with the plot in Fig. 3. However, we observe a reduction in lifetime when the dephasing is introduced. Although the lifetime follows a staircase pattern, the lifetime where the plateaus occur are reduced. Further, the reduction is not linear as a function of dephasing strength. We find that for $\gamma_\phi/K = 10^{-6}$, the lifetime plot (dotted red curve) runs very close to the plot for $\gamma_\phi = 0$. However, the lifetime gets drastically reduced for ten fold increase

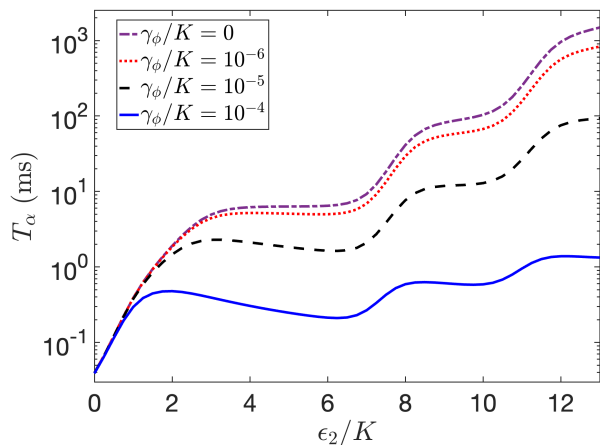


Figure 7. T_α as a function of the two-photon drive strength ϵ_2/K in the presence and absence of dephasing for different values of γ_ϕ . We use the same parameters as in Fig. 3.

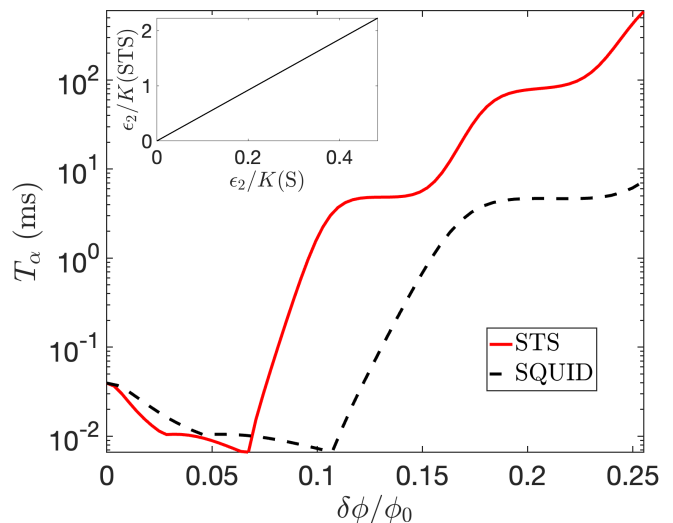


Figure 8. T_α as a function of the modulation depth for a single SQUID (black dashed curve) compared to the case of STS (solid red curve) for $K/h = 31.3$ MHz, ϕ_0 is the flux quantum. In the inset, we plot the two-photon drive strength obtained for the STS compared to a SQUID (S) by varying the modulation depth.

in the dephasing strength (black dashed curve). The reduction is even more significant for $\gamma_\phi/K = 10^{-4}$ (solid blue curve) to the point that the lifetime for the two-photon drive strength $\epsilon_2/K \approx 2$ is almost the same as for the two-photon drive strength $\epsilon_2/K \approx 10$.

B. Comparison with SQUID based Kerr-cat

In this section, we will study the SQUID based Kerr-cat qubit and compare its robustness against a STS Kerr-cat qubit. In order to realize a Kerr-cat qubit, we pump a capacitor shunted SQUID with an external flux, $\phi_e = \pi/4 + \delta\phi \cos(\omega_d t)$ (see Appendix C for details). The pumping is done around $\pi/4$ since unlike STS, a single SQUID behaves as a capacitor at $\pi/2$. Doing so, we obtain the following static effective Hamiltonian up to $\mathcal{O}(\varphi_{zps}^4)$

$$\hat{\mathcal{H}}_{\text{SQ}} = \tilde{\Delta} \hat{a}^\dagger \hat{a} + \tilde{\epsilon}_2 (\hat{a}^{\dagger 2} + \hat{a}^2) - \tilde{K} \hat{a}^{\dagger 2} \hat{a}^2 + \tilde{\Lambda} (\hat{a}^{\dagger 3} \hat{a} + \hat{a}^\dagger \hat{a}^3) + \tilde{\Theta} (\hat{a}^{\dagger 4} + \hat{a}^4), \quad (14)$$

where for a single junction SQUID $\tilde{K} = E_C/2$, $\tilde{\epsilon}_2 = -\frac{\delta\phi}{2\sqrt{2}} (\sqrt{2E_C E_J} - E_C) + \delta\phi^3 E_C E_J / 4\omega_d$ (for the details of the calculations and for the dependence of $\tilde{\Delta}$, $\tilde{\Lambda}$ and $\tilde{\Theta}$ on the circuit parameters, see Appendix C).

The two significant differences between the single SQUID Kerr-cat Hamiltonian and the STS Hamiltonian in

	SQUID	SNAIL[13]	STS
Drive	Flux	Charge	Flux
RWA	$\mathcal{O}(\varphi_{zps}^0)$	$\mathcal{O}(\varphi_{zps}^0)$	$\mathcal{O}(\varphi_{zps}^0)$
Two photon dissipation	$\mathcal{O}(\varphi_{zps}^3)$ $\propto E_{J\Delta}$	$\mathcal{O}(\varphi_{zps}^1)$ $\propto g_3$	$\mathcal{O}(\varphi_{zps}^3)$ $\propto E_{J\Delta}$
ϵ_2	$-\frac{\delta\phi}{2\sqrt{2}}E_{J\Sigma}\varphi_{zps}^2$	$g_3\frac{4\Omega_d}{3\omega_d}$	$\frac{\delta\phi}{2}E_{J\Sigma}\varphi_{zps}^2$
K	$E_C/2$	$-\frac{3g_4}{2} + \frac{10g_3^2}{3\omega_d}$	$E_C/2$
T_α (ms)	188 μ s	2.58 μ s	1.22 ms

Table I. Comparison of three different circuit designs for Kerr-cat qubit. Ω_d is the periodic drive strength and g_m is the m -th order nonlinearity coefficient in the SNAIL Hamiltonian [13]. We compare only the leading order contributions. The lifetime T_α was calculated for $\epsilon_2 = 8K$ (for STS and SNAIL) and $K = 14.4$ MHz (see Fig. 12). The two-photon drive strength for the single SQUID, $\tilde{\epsilon} = -\epsilon_2/\sqrt{2}$.

Eq. (7) is the negative sign in front of the two-photon drive strength $\tilde{\epsilon}_2$ and the final quartic term in \hat{a} and \hat{a}^\dagger which is absent in the STS case. However, $\tilde{\Theta}$ is proportional to $\sim \varphi_{zps}^4/100$ giving a negligible contribution for a sufficiently diluted Kerr coefficient. Comparing the Kerr and two-photon driving strength with the STS case, we find $\tilde{K} = K$ and $\tilde{\epsilon}_2 = -\epsilon_2/\sqrt{2}$ up to the leading order in zero point phase spread. Note that, when all the parameters are considered same, the Kerr coefficient for the SQUID is the same as the Kerr coefficient for the STS whereas the two-photon drive for the same value of modulation depth is largely reduced compared to the STS (see the inset of Fig. 8). This results in a reduced T_α for SQUID in comparison to the STS as shown in Fig. 8. In Table I, we compare different properties of the three different proposed designs of the Kerr-cat qubit, namely the SQUID, SNAIL and STS designs. Note that the two photon dissipation which enters at $\mathcal{O}(\varphi_{zps}^1)$ for the SNAIL design only gets introduced at $\mathcal{O}(\varphi_{zps}^3)$ for SQUID designs. This leads to robust T_α for the STS design even in the high Kerr limit in contrast to the SNAIL (see Appendix D for details).

C. Qubit Initialization

As we have observed, Kerr-cat qubits with finite detuning have enhanced T_α compared to the counterpart with no detuning. Taking into account the extra detuning introduced by the drive dependent detuning term Λ , T_α peaks were observed for values of Δ slightly larger than $2mK$, where m is a non-negative even integer (see Fig. 6 (a)). In the absence of detuning, the cat states are the eigenstates of the Kerr-cat Hamiltonian. Hence,

the qubit can be initialized by adiabatically driving the two-photon drive strength (ϵ_2) from zero to some finite value. However, for a detuned Kerr-cat qubit, the energy eigenstates of the initial Fock states $|n\rangle$ are expressed by $E_n = [cn - n(n-1)]K$ where detuning is expressed by $\Delta = cK$, for any constant c . When there is a sufficient detuning, the $|0\rangle$ and $|1\rangle$ states will not be the ground states of Fock Hamiltonian, while the cat states are still the ground states of the detuned Kerr-cat Hamiltonian. This prevents the evolution of the $|0\rangle$ and $|1\rangle$ states to the cat states through adiabatic driving. In this section, we will discuss on how to initialize the cat qubit using single photon dissipation and readout.

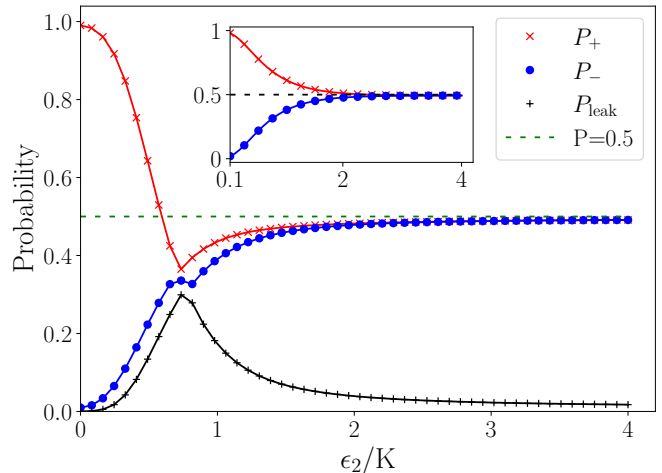


Figure 9. The steady state probability of getting the eigenstates (red curve with cross for $|+\rangle$, blue curve with dots for $|-\rangle$) and the leakage probability $P_{\text{leak}} = 1 - P_+ - P_-$ (black curve with plus) as a function of the two-photon drive strength ϵ_2 for detuning $\Delta = 2.1K$. In the inset, we plot the $\Delta = 0$ case. We considered the single photon loss rate, $\gamma = 0.05K$ and the Bose-Einstein distribution, $n_{\text{th}} = 0.01$.

In Fig. 9, in the absence of a drive ($\epsilon_2 = 0$) the qubit is in the Fock space and hence, the red and blue curves represent the eigenstates $|0\rangle$ and $|1\rangle$, respectively. If we look at the weak two-photon drive regime for ϵ_2/K between 0 and 2, we observe a finite leakage probability $P_{\text{leak}} = 1 - P_+ - P_-$ (black curve), where P_+ (red curve) and P_- (blue curve) are the probabilities of obtaining the first two eigenstates when the eigenenergies are sorted from high to low. These eigenstates correspond to the cat states in the absence of detuning (the inset of Fig. 9 where the leakage probability is zero even for weak two photon drive). For $\epsilon_2 \approx 0$, the off-diagonal terms in the Hamiltonian are very small in the Fock basis. Hence, the probabilities are mostly determined by n_{th} . However, for small but finite two-photon drive, $0 < \epsilon_2 \leq \Delta$, when the first two eigenstates are not degenerate, the contribution from the off-diagonal elements and the thermal contribution compete to give finite leakage probability. Further, when $\epsilon_2 \gg \Delta$, the first two eigenstates become degenerate leading to the convergence of the blue and red curves

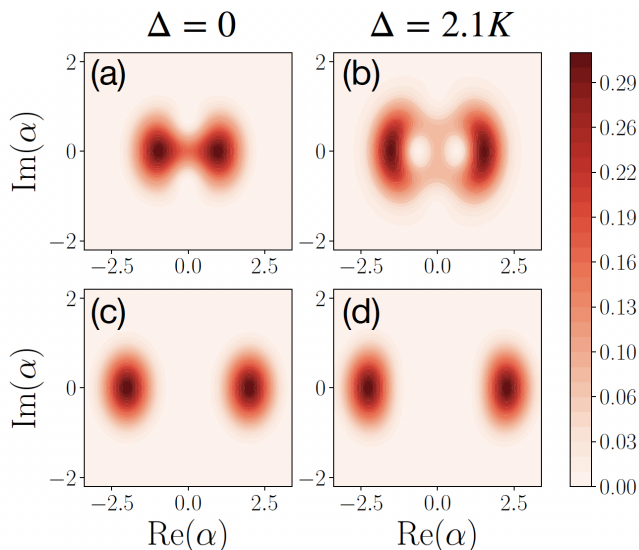


Figure 10. Wigner function plot for $\epsilon_2 = K$ ((a) and (b)) and for $\epsilon_2 = 4K$ ((c) and (d)) for two different values of detuning. We considered the single photon loss rate, $\gamma = 0.05K$ and the Bose-Einstein distribution, $n_{\text{th}} = 0.01$.

to the steady state probability $P = 0.5$. Hence, in the presence of strong two-photon drive and single photon dissipation, the state $|0\rangle$ and $|1\rangle$ relax to a classical mixture of the first two eigenstates ($|+\rangle$ and $|-\rangle$) with equal probability in the steady state.

In Fig. 10, we show the Wigner plots for the detuned and non-detuned qubits at different drive strengths. We can see that at weak drive, $\epsilon_2 = K$, coherent states are not stabilized enough to be fully separated in both Figs. 10 (a) and (b). However, in the detuned case in Fig. 10 (b), the coherent states seem to be more distorted than the non-detuned case in Fig. 10 (a). On the other hand, for strong drive, $\epsilon_2 = 4K$, we can see in both Figs. 10 (c) and (d) that the coherent states are fully separated and have equal probability. This supports our previous argument in Fig. 9: for a strong enough two photon drive and long enough relaxation time, regardless of the detuning, we get a classical mixture of coherent states $|\pm\alpha\rangle$ at equal steady state probability.

Consequently, we can initialize the detuned Kerr-cat qubit (that satisfies the drive and relaxation criteria men-

tioned previously) by performing a readout along the qubit's z -axis and preparing it in the coherent state $|\pm\alpha\rangle$, based on the outcome of the readout. Finally, it is important to distinguish that the initialization time of a detuned Kerr-cat qubit depends strongly on the relaxation time rather than the ramp time of the two photon drive, unlike the non-detuned case.

V. CONCLUSION

In this article, we proposed an alternate circuit based on STS as next generation Kerr-cat qubits. We then calculated the static effective Hamiltonian and static effective master equation for the proposed design. The Hamiltonian and the master equation were calculated considering strong driving $\hbar\omega_d \approx 2\epsilon_c$ with weak modulation depth $\delta\phi \ll 1$, weak system-environment coupling and small charging energy $E_C \ll E_J$. Under the above conditions and including some dephasing, we observed that T_α of the proposed design can reach 100 ms. Unlike the SNAIL Kerr-cat where the two photon heating terms drastically reduces the lifetime, we found that the two-photon effects enter only through SQUID asymmetry and have a negligible effect on the lifetime in the case of STS. The multi-photon effects are dominant for large Kerr coefficient, however, the Kerr coefficient can be diluted considering multiple STS in series. We also investigated the dependence of lifetime on dephasing and found a non-monotonous relation between the reduction of lifetime and dephasing strength. We also compared the lifetime of the proposed design with the SQUID Kerr-cat. If we keep all the other parameters same, we find that the Kerr coefficient for the SQUID remains the same whereas the two-photon drive strength is reduced leading to a significant reduction in lifetime. We also discussed on a method to initialize detuned cat qubits employing single photon dissipation and readout.

VI. ACKNOWLEDGEMENT

We thank Jayameenakshi Venkatraman, Michel Devoret and Tathagata Karmakar for valuable discussions. This work was supported by the U. S. Army Research Office under grant W911NF-22-1-0258.

Appendix A: STS - Hamiltonian

We consider the STS circuit shown in Fig. 1, where three Josephson junctions J_i , $i = 1, 2, 3$ are placed in parallel to each other. The STS is shunted by a capacitor of capacitance C_T . The Josephson energy associated with the junction J_i is given by E_{J_i} . Moreover, C_i gives the self-capacitance of the junction J_i . Following Ref. [22], the Hamiltonian for

the circuit can be written as

$$\hat{H}_{\text{lab}} = 4E_C \hat{n}^2 - E_{J1} \cos \left(\hat{\varphi} + \frac{C_2 + C_3}{C_\Sigma} \phi_e + \frac{C_3}{C_\Sigma} \phi'_e \right) - E_{J2} \cos \left(\hat{\varphi} - \frac{C_1}{C_\Sigma} \phi_e + \frac{C_3}{C_\Sigma} \phi'_e \right) - E_{J3} \cos \left(\hat{\varphi} - \frac{C_1}{C_\Sigma} \phi_e - \frac{C_1 + C_2}{C_\Sigma} \phi'_e \right), \quad (\text{A1})$$

where $C_\Sigma = C_1 + C_2 + C_3$ and the charging energy, $E_C = e^2/2C$, $C = C_\Sigma + C_T$. $\phi_e, \phi'_e, i = 1, 2$ gives the external flux threading the two SQUID loops in units of the flux quantum, $\phi_0 = h/2e$. The canonical variables $\hat{\varphi}$ and \hat{n} are the phase and charge operators which satisfy the commutation relation, $[\hat{\varphi}, \hat{n}] = i$, where i is the imaginary unit. In our analysis, we will consider equal self-capacitances for each Josephson junction, i.e. $C_1 = C_2 = C_3$. The Hamiltonian reduces to

$$\hat{H}_{\text{lab}} = 4E_C \hat{n}^2 - E_{J1} \cos \left(\hat{\varphi} + \frac{2}{3} \phi_e + \frac{1}{3} \phi'_e \right) - E_{J2} \cos \left(\hat{\varphi} - \frac{1}{3} \phi_e + \frac{1}{3} \phi'_e \right) - E_{J3} \cos \left(\hat{\varphi} - \frac{1}{3} \phi_e - \frac{2}{3} \phi'_e \right). \quad (\text{A2})$$

Taking $\phi_e = \phi'_e = \phi_e$ along with $E_{J\Sigma} = (E_{J1} + E_{J3})/2$ and $E_{J\Delta} = (E_{J1} - E_{J3})/2$, the Hamiltonian becomes

$$\hat{H}_{\text{lab}} = 4E_C \hat{n}^2 - E_{J2} \cos \hat{\varphi} - 2E_{J\Sigma} \cos \phi_e \cos \hat{\varphi} + 2E_{J\Delta} \sin \phi_e \sin \hat{\varphi}, \quad (\text{A3})$$

where the first two terms on the right hand side represent a transmon and the last two terms a driven SQUID. Hence, under the approximations considered, a STS circuit is equivalent to having a SQUID and a transmon sharing the same node. For symmetric junctions, one gets contributions that are even order in the phase operator contributions whereas the junction asymmetry leads to odd orders. We take the external flux drive of the form, $\phi_e = -\frac{\pi}{2} + \delta\varphi \cos(\omega_d t)$, where the DC bias $-\pi/2$ is chosen so as to attain highest first-order sensitivity to the modulation depth while removing the parasitic even harmonics of the drive. The even harmonics of the drive do enter through the asymmetric SQUID term (last term in Eq. (A3)) however its effect can be mitigated by making the SQUID junctions as symmetric as possible. The Hamiltonian in Eq. (A3) reduces

$$\hat{H}_{\text{lab}} = 4E_C \hat{n}^2 - E_{J2} \cos \hat{\varphi} - 2E_{J\Sigma} \sin(\delta\phi \cos(\omega_d t)) \cos \hat{\varphi} - 2E_{J\Delta} \cos(\delta\phi \cos(\omega_d t)) \sin \hat{\varphi} \quad (\text{A4})$$

We can represent the first two terms on the right hand side of the above Hamiltonian as the transmon Hamiltonian ($\hat{H}_{\text{lab,T}}$), the next two terms as symmetric SQUID Hamiltonian ($\hat{H}_{\text{lab,SQ}}^{\text{sym}}$) and final two terms as the asymmetric SQUID contribution ($\hat{H}_{\text{SQ}}^{\text{lab,asym}}$). Hence,

$$\hat{H}_{\text{lab}} = \hat{H}_{\text{lab,T}} + \hat{H}_{\text{lab,SQ}}^{\text{sym}} + \hat{H}_{\text{lab,SQ}}^{\text{asym}} \quad (\text{A5})$$

Using $\hat{\varphi} = \varphi_{\text{zps}}(\hat{a}^\dagger + \hat{a})$ and $\hat{n} = -i(\hat{a} - \hat{a}^\dagger)/(2\varphi_{\text{zps}})$, where $\varphi_{\text{zps}} = (2E_C/E_{J2})^{1/4}$ is the zero point spread of the phase operator around the Josephson junction and $\hat{a}(\hat{a}^\dagger)$ is the bosonic annihilation(creation) operator, we obtain

$$\hat{H}_{\text{lab,T}} = \epsilon_c \hat{a}^\dagger \hat{a} - K \hat{a}^{\dagger 2} \hat{a}^2, \quad (\text{A6})$$

where $\epsilon_c = \sqrt{8E_C E_{J2}}$ and $K = E_C/2$. Similarly, the symmetric SQUID Hamiltonian can be written as

$$\hat{H}_{\text{lab,SQ}}^{\text{sym}} = -2E_{J\Sigma} \sin(\delta\phi \cos(\omega_d t)) \sum_{n=1,2} \frac{(-1)^n}{(2n)!} [\varphi_{\text{zps}}(\hat{a} + \hat{a}^\dagger)]^{2n}. \quad (\text{A7})$$

We will seek for a static effective Hamiltonian under the condition $\hbar\omega_d \approx 2\epsilon_c$. Going to rotating frame of the qubit defined through $a \rightarrow ae^{-i\epsilon_c t/\hbar}$ and $\hat{H}_{\text{lab}} \rightarrow \hat{H}_T + \hat{H}_{\text{SQ}}^{\text{sym}} + \hat{H}_{\text{SQ}}^{\text{asym}}$, we obtain

$$\hat{H}_T = \delta \hat{a}^\dagger \hat{a} - K \hat{a}^{\dagger 2} \hat{a}^2, \quad (\text{A8})$$

and

$$\hat{H}_{\text{SQ}}^{\text{sym}} = -2E_{J\Sigma} \sin(\delta\phi \cos(\omega_d t)) \sum_{n=1,2} \frac{(-1)^n}{(2n)!} \left[\varphi_{\text{zps}}(\hat{a}e^{-i\omega_d t/2} + \hat{a}^\dagger e^{i\omega_d t/2}) \right]^{2n}, \quad (\text{A9})$$

where $\delta = \epsilon_c - \hbar\omega_d/2$. For weak modulation depth such that $\delta\phi \approx \varphi_{\text{zps}}$, we can make the following approximation, $\sin(\delta\phi \cos(\omega_d t)) \approx \delta\phi \cos(\omega_d t)$. Doing so, we will keep only up to $\mathcal{O}(\varphi_{\text{zps}}^4)$ contributions in our Hamiltonian and master equation calculations. The symmetric SQUID Hamiltonian reduces to

$$\hat{H}_{\text{SQ}}^{\text{sym}} = \sum_{n=2,4} G_{n,S} (e^{i\omega_d t} + e^{-i\omega_d t}) \left(\hat{a} e^{-i\omega_d t/2} + \hat{a}^\dagger e^{i\omega_d t/2} \right)^n, \quad (\text{A10})$$

where $G_{2,S} = \delta\varphi E_{\text{J}\Sigma} \varphi_{\text{zps}}^2/2$ and $G_{4,S} = -\delta\varphi E_{\text{J}\Sigma} \varphi_{\text{zps}}^4/24$. Now, the asymmetric SQUID contribution in Eq. (A5) can be written as

$$\hat{H}_{\text{SQ}}^{\text{asym}} = -2E_{\text{J}\Delta} \left[1 - \delta\phi^2 \cos^2(\omega_d t)/2 \right] \sin \hat{\varphi}, \quad (\text{A11})$$

where we made the following approximation, $\cos(\delta\phi \cos(\omega_d t)) \approx 1 - \delta\phi^2 \cos^2(\omega_d t)/2$. Similar to the symmetric case, we will keep only up to $\mathcal{O}(\varphi_{\text{zps}}^4)$ terms in our calculations. Taylor expanding $\sin \hat{\varphi}$, we obtain

$$\hat{H}_{\text{SQ}}^{\text{asym}} = -2E_{\text{J}\Delta} \left[\left(1 - \frac{\delta\phi^2}{4} \right) - \frac{\delta\phi^2}{8} (e^{2i\omega_d t} + e^{-2i\omega_d t}) \right] \left(\hat{\varphi} - \frac{\hat{\varphi}^3}{3!} \right) \quad (\text{A12})$$

Using $\hat{\varphi} = \varphi_{\text{zps}}(\hat{a}^\dagger + \hat{a})$ and going to the rotating frame (see Eq. (A9) for reference), we obtain

$$\begin{aligned} \hat{H}_{\text{SQ}}^{\text{asym}} = -2E_{\text{J}\Delta} \left[\left(1 - \frac{\delta\phi^2}{4} \right) - \frac{\delta\phi^2}{8} (e^{2i\omega_d t} + e^{-2i\omega_d t}) \right] \\ \left[\varphi_{\text{zps}} (\hat{a}^\dagger e^{i\omega_d t/2} + \hat{a} e^{-i\omega_d t/2}) - \frac{\varphi_{\text{zps}}^3}{3!} (\hat{a}^\dagger e^{i\omega_d t/2} + \hat{a} e^{-i\omega_d t/2})^3 \right]. \end{aligned} \quad (\text{A13})$$

Since we consider $\delta\phi \sim \varphi_{\text{zps}}$, terms containing $\varphi_{\text{zps}}^3 \delta\phi^2$ would have an order comparable to φ_{zps}^5 , which can then be dropped. If we drop all of these terms, we get

$$\begin{aligned} \hat{H}_{\text{SQ}}^{\text{asym}} = -2E_{\text{J}\Delta} \left[\left(1 - \frac{\delta\phi^2}{4} \right) - \frac{\delta\phi^2}{8} (e^{2i\omega_d t} + e^{-2i\omega_d t}) \right] \\ \left[\varphi_{\text{zps}} (\hat{a}^\dagger e^{i\omega_d t/2} + \hat{a} e^{-i\omega_d t/2}) \right] + 2E_{\text{J}\Delta} \left[\frac{\varphi_{\text{zps}}^3}{3!} (\hat{a}^\dagger e^{i\omega_d t/2} + \hat{a} e^{-i\omega_d t/2})^3 \right]. \end{aligned} \quad (\text{A14})$$

We can rewrite the above Hamiltonian as

$$\hat{H}_{\text{SQ}}^{\text{asym}} = \left(G_{1,S} + \tilde{G}_{1,S} (e^{2i\omega_d t} + e^{-2i\omega_d t}) \right) (\hat{a}^\dagger e^{i\omega_d t/2} + \hat{a} e^{-i\omega_d t/2}) + G_{3,S} (\hat{a}^\dagger e^{i\omega_d t/2} + \hat{a} e^{-i\omega_d t/2})^3, \quad (\text{A15})$$

where $G_{1,S} = -2E_{\text{J}\Delta} \varphi_{\text{zps}} (1 - \delta\phi^2/4)$, $\tilde{G}_{1,S} = E_{\text{J}\Delta} \varphi_{\text{zps}} \delta\phi^2/4$ and $G_{3,S} = E_{\text{J}\Delta} \varphi_{\text{zps}}^3/3$.

1. Dilution of Kerr coefficient

As shown in Fig. 11, we consider M number of identical STS coupled in series. Each STS has \tilde{N} number of identical junctions in the trasmon branch. We argue that the circuit is only a function of a single degree of freedom $\hat{\varphi}$ although it consists of $M(\tilde{N} + 2)$ Josephson junctions. This can be done since the plasma frequency $\Omega_p = \sqrt{8E_{\text{J}}E_{\text{C}_j}}/h$, where E_{C_j} is the charging energy associated with the junction capacitance C_j , is sufficiently higher than the frequency at which the dynamics we are interested in occurs. In this case, the dynamics coming from the extra degrees of freedom pertaining to each Josephson junctions will oscillate fast compared to that of the mode $\hat{\varphi}$ and can be integrated out [43]. The Hamiltonian is given by

$$\hat{H}_{\text{lab}} = \hat{H}_{\text{lab}}^{\text{sym}} = 4E'_C \hat{n}^2 - NE'_{\text{J}2} \cos \frac{\hat{\varphi}}{N} - 2ME'_j \cos \phi_e \cos \frac{\hat{\varphi}}{M}, \quad (\text{A16})$$

where $E'_C \approx E_C$ due to the large trasmon capacitance and $N = M\tilde{N}$. Taylor expanding the sine and cosine up to fourth order in φ_{zps} for the phase operators and dropping scalars gives

$$\hat{H}_{\text{lab}}^{\text{sym}} = 4E_C \hat{n}^2 + NE'_{\text{J}2} \left[\frac{1}{2!} \left(\frac{\hat{\varphi}}{N} \right)^2 - \frac{1}{4!} \left(\frac{\hat{\varphi}}{N} \right)^4 \right] + 2ME'_j \cos \phi_e \left[\frac{1}{2!} \left(\frac{\hat{\varphi}}{M} \right)^2 - \frac{1}{4!} \left(\frac{\hat{\varphi}}{M} \right)^4 \right]. \quad (\text{A17})$$

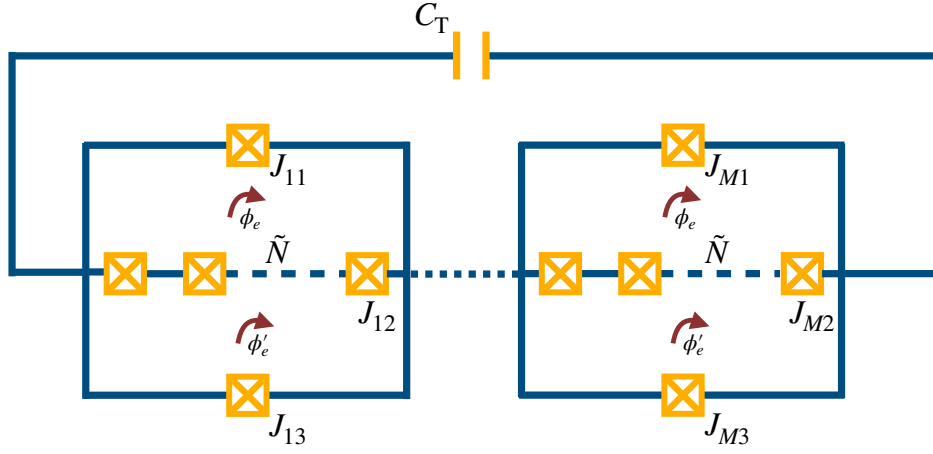


Figure 11. Multiple STS circuits in series.

If we set $E_{J2} = \frac{E'_{J2}}{N}$ and $E_J = \frac{E'_J}{M}$, we can rewrite the Hamiltonian in terms of E_{J2} and E_J as

$$\hat{H}_{\text{lab}}^{\text{sym}} = 4E_C \hat{n}^2 + E_{J2} \left[\frac{\hat{\varphi}^2}{2!} - \frac{1}{4!} \left(\frac{\hat{\varphi}^2}{N} \right)^2 \right] + 2E_J \cos \phi_e \left[\frac{\hat{\varphi}^2}{2!} - \frac{1}{4!} \left(\frac{\hat{\varphi}^2}{M} \right)^2 \right]. \quad (\text{A18})$$

We note that this is the same form as with the single junction case, except that the fourth order φ_{zps} terms now have an extra $\frac{1}{M^2}$ or $\frac{1}{N^2}$ factor. The new expressions for the zero point phase spread, Kerr coefficient and two-photon drive strength are

$$\varphi_{\text{zps}} = \left(\frac{2E_C}{E_{J2}} \right)^{\frac{1}{4}} = N^{\frac{1}{4}} \varphi'_{\text{zps}}, \quad (\text{A19})$$

$$K = -\frac{E_{J2} \varphi_{\text{zps}}^4}{4N^2} = \frac{K'}{N^2}, \quad (\text{A20})$$

$$G_{2,S} = \frac{\delta\varphi}{2} E_J \varphi_{\text{zps}}^2 = \frac{\sqrt{N}}{M} G'_{2,S}, \quad (\text{A21})$$

and

$$G_{4,S} = -\frac{\delta\varphi E'_J \varphi_{\text{zps}}^4}{24M^2} = \frac{N}{M^3} G'_{4,S}. \quad (\text{A22})$$

2. Static effective Hamiltonian

The STS Hamiltonian (which includes contribution from transmon, the symmetric and asymmetric part of SQUID) takes the following form

$$\begin{aligned} \hat{H} = & \delta \hat{a}^\dagger \hat{a} - K \hat{a}^{\dagger 2} \hat{a}^2 + \sum_{n=2,4} G_{n,S} (e^{i\omega_d t} + e^{-i\omega_d t}) \left(\hat{a} e^{-i\omega_d t/2} + \hat{a}^\dagger e^{i\omega_d t/2} \right)^n \\ & + \left(G_{1,S} + \tilde{G}_{1,S} (e^{2i\omega_d t} + e^{-2i\omega_d t}) \right) (\hat{a}^\dagger e^{i\omega_d t/2} + \hat{a} e^{-i\omega_d t/2}) + G_{3,S} (\hat{a}^\dagger e^{i\omega_d t/2} + \hat{a} e^{-i\omega_d t/2})^3. \end{aligned} \quad (\text{A23})$$

The time-independent part of the STS Hamiltonian is given by

$$\hat{H}_{\text{st}} = \delta \hat{a}^\dagger \hat{a} - K \hat{a}^{\dagger 2} \hat{a}^2 + (G_{2,S} + 6G_{4,S}) (\hat{a}^2 + \hat{a}^{\dagger 2}) + 4G_{4,S} (\hat{a}^{\dagger 3} \hat{a} + \hat{a}^\dagger \hat{a}^3). \quad (\text{A24})$$

We will break the time-dependent part of the total Hamiltonian into different orders in φ_{zps} contributions:

$$\begin{aligned}
\text{osc} \left(\hat{H}^{(1)}(t) \right) &= \left(G_{1,S} + \tilde{G}_{1,S} (e^{2i\omega at} + e^{-2i\omega at}) \right) \hat{a} e^{-i\omega at/2} + \text{h.c.}, \\
\text{osc} \left(\hat{H}^{(2)}(t) \right) &= G_{2,S} \left((e^{i\omega at} + e^{-i\omega at}) \hat{a}^\dagger \hat{a} + e^{-2i\omega at} \hat{a}^2 \right) + \text{h.c.}, \\
\text{osc} \left(\hat{H}^{(3)}(t) \right) &= G_{3,S} \left(3e^{-i\omega at/2} \hat{a} + e^{-3i\omega at/2} \hat{a}^3 + 3e^{-i\omega at/2} \hat{a}^\dagger \hat{a}^2 \right) + \text{h.c.}, \\
\text{osc} \left(\hat{H}^{(4)}(t) \right) &= G_{4,S} \left(6(e^{i\omega at} + e^{-i\omega at}) \hat{a}^\dagger \hat{a} + 6e^{-2i\omega at} \hat{a}^2 + (e^{-i\omega at} + e^{-3i\omega at}) \hat{a}^4 + 3(e^{i\omega at} + e^{-i\omega at}) \hat{a}^\dagger \hat{a}^2 \right) + \text{h.c.},
\end{aligned} \tag{A25}$$

where $\hat{H}^{(i)}$ represent the $\mathcal{O}(\varphi_{zps}^i)$ contribution. $\text{osc}(g(t)) = g(t) - \int_0^T g(t) dt$ is the oscillating part of g ; T is the periodicity of $g(t)$. While writing Eqs. (A25), we neglected all the scalar terms. The first and third order terms originate from $\hat{H}_{SQ}^{\text{asym}}$ whereas the second and the fourth order terms originate from $\hat{H}_{SQ}^{\text{sym}}$.

We follow Ref. [45] to obtain a time-independent Hamiltonian at different orders of φ_{zps} using a generalized Schieffer-Wolf transformation. The canonical transformation that leads to an effective time-independent Hamiltonian is given by

$$\hat{\mathcal{H}} = e^{\hat{L}_S} (\hat{H}) + \int_0^1 d\epsilon e^{\epsilon \hat{L}_S} (\dot{\hat{S}}(t)), \tag{A26}$$

where $\hat{S}(t)$ is the generator of the transformation and $\hat{L}_S(\hat{O}(t)) = \frac{1}{i\hbar} [\hat{S}(t), \hat{O}(t)]$, where $\hat{O}(t)$ can be any operator. Expanding the above equation, we find following expressions for the total system Hamiltonian at different orders of φ_{zps}

$$\begin{aligned}
\hat{\mathcal{H}}^{(0)} &= 0 \quad \text{since } \hat{H}^{(0)} = 0, \\
\hat{\mathcal{H}}^{(1)} &= \hat{H}^{(1)}(t) + \partial_t \hat{S}^{(1)}, \\
\hat{\mathcal{H}}^{(2)} &= \hat{H}^{(2)}(t) + \frac{1}{i\hbar} [\hat{S}^{(1)}, \hat{H}^{(1)}] + \frac{1}{2i\hbar} [\hat{S}^{(1)}, \partial_t \hat{S}^{(1)}] + \partial_t \hat{S}^{(2)}, \\
\hat{\mathcal{H}}^{(3)} &= \hat{H}^{(3)}(t) + \frac{1}{i\hbar} [\hat{S}^{(1)}, \hat{H}^{(2)}] + \frac{1}{i\hbar} [\hat{S}^{(2)}, \hat{H}^{(1)}] + \frac{1}{2!(i\hbar)^2} [\hat{S}^{(1)}, [\hat{S}^{(1)}, \hat{H}^{(1)}]] \\
&\quad + \frac{1}{2i\hbar} \left([\hat{S}^{(1)}, \partial_t \hat{S}^{(2)}] + [\hat{S}^{(2)}, \partial_t \hat{S}^{(1)}] \right) + \frac{1}{3!(i\hbar)^2} [\hat{S}^{(1)}, [\hat{S}^{(1)}, \partial_t \hat{S}^{(1)}]] + \partial_t \hat{S}^{(3)},
\end{aligned} \tag{A27}$$

and

$$\begin{aligned}
\hat{\mathcal{H}}^{(4)} &= \hat{H}^{(4)} + [\hat{S}^{(1)}, \hat{H}^{(3)}] + [\hat{S}^{(2)}, \hat{H}^{(2)}] + [\hat{S}^{(3)}, \hat{H}^{(1)}] + \frac{1}{2!(i\hbar)^2} \left([\hat{S}^{(1)}, [\hat{S}^{(1)}, \hat{H}^{(2)}]] + [\hat{S}^{(1)}, [\hat{S}^{(2)}, \hat{H}^{(1)}]] \right) \\
&\quad + [\hat{S}^{(2)}, [\hat{S}^{(1)}, \hat{H}^{(1)}]] + \frac{1}{3!(i\hbar)^3} [\hat{S}^{(1)}, [\hat{S}^{(1)}, [\hat{S}^{(1)}, \hat{H}^{(1)}]]] + \frac{1}{2i\hbar} \left([\hat{S}^{(1)}, \partial_t \hat{S}^{(3)}] + [\hat{S}^{(2)}, \partial_t \hat{S}^{(2)}] + [\hat{S}^{(3)}, \partial_t \hat{S}^{(1)}] \right) \\
&\quad + \frac{1}{3!(i\hbar)^2} \left([\hat{S}^{(1)}, [\hat{S}^{(1)}, \partial_t \hat{S}^{(2)}]] + [\hat{S}^{(1)}, [\hat{S}^{(2)}, \partial_t \hat{S}^{(1)}]] + [\hat{S}^{(2)}, [\hat{S}^{(1)}, \partial_t \hat{S}^{(1)}]] \right) + \partial_t \hat{S}^{(4)},
\end{aligned} \tag{A28}$$

where we expanded $\hat{S}(t) = \sum_n \hat{S}^{(n)}(t)$ at different orders of φ_{zps} and we choose

$$\begin{aligned}
\hat{S}^{(1)}(t) &= - \int dt \text{osc} \left(\hat{H}^{(1)}(t) \right), \\
\hat{S}^{(2)}(t) &= - \int dt \text{osc} \left(\hat{H}^{(2)}(t) + \frac{1}{i\hbar} [\hat{S}^{(1)}(t), \hat{H}^{(1)}(t)] + \frac{1}{2i\hbar} [\hat{S}^{(1)}(t), \partial_t \hat{S}^{(1)}(t)] \right),
\end{aligned} \tag{A29}$$

and so on. Note that all the terms in $H^{(n)}(t)$ are time-dependent. The time independent terms were all added to Eq. (A24). We find,

$$\hat{S}^{(1)} = \frac{2i}{\omega_d} e^{i\omega at/2} \left[G_{1,S} (\hat{a}^\dagger - \hat{a} e^{-i\omega at}) + \tilde{G}_{1,S} \hat{a}^\dagger \left(\frac{1}{5} e^{2i\omega at} - \frac{1}{3} e^{-2i\omega at} \right) + \tilde{G}_{1,S} \hat{a} \left(\frac{1}{3} e^{i\omega at} - \frac{1}{5} e^{-3i\omega at} \right) \right]. \tag{A30}$$

For $\hat{S}^{(2)}$, we obtain

$$\hat{S}^{(2)}(t) = \frac{iG_{2,S}}{2\omega_d} (\hat{a}^{\dagger 2} e^{2i\omega_d t} - \hat{a}^2 e^{-2i\omega_d t}) + \frac{2iG_{2,S}}{\omega_d} \hat{a}^{\dagger} \hat{a} (e^{i\omega_d t} - e^{-i\omega_d t}) + \text{cons.} \quad (\text{A31})$$

Similarly, at $\mathcal{O}(\varphi_{zps}^3)$ we have

$$\hat{S}^{(3)}(t) = - \int dt \text{osc} \left(\hat{H}^{(3)}(t) + \frac{1}{i\hbar} [\hat{S}^{(1)}, \hat{H}^{(2)}] + \frac{1}{i\hbar} [\hat{S}^{(2)}, \hat{H}^{(1)}] + \frac{1}{2i\hbar} \left([\hat{S}^{(1)}, \partial_t \hat{S}^{(2)}] + [\hat{S}^{(2)}, \partial_t \hat{S}^{(1)}] \right) \right), \quad (\text{A32})$$

where we used $[\hat{S}^{(1)}, [\hat{S}^{(1)}, \hat{H}^{(1)}]] = 0$ and $[\hat{S}^{(1)}, [\hat{S}^{(1)}, \partial_t \hat{S}^{(1)}]] = 0$. Since,

$$- \int dt \text{osc} \left(H^{(3)}(t) \right) = \frac{6iG_{3,S}}{\omega_d} \left(e^{i\omega_d t/2} (\hat{a}^{\dagger} + \hat{a}^{\dagger 2} \hat{a}) - e^{-i\omega_d t/2} (\hat{a} + \hat{a}^2 \hat{a}^{\dagger}) \right) + \frac{2iG_{3,S}}{3\omega_d} \left(e^{3i\omega_d t/2} \hat{a}^{\dagger 3} - e^{-3i\omega_d t/2} \hat{a}^3 \right), \quad (\text{A33})$$

we find

$$\begin{aligned} \hat{S}^{(3)}(t) = \mathcal{G}_{31}(t) \hat{a}^{\dagger} + \mathcal{G}_{31}^{\dagger}(t) \hat{a} + \frac{2i}{3\omega_d} G_{3,S} e^{3i\omega_d t/2} \hat{a}^{\dagger} \hat{a}^{\dagger} \hat{a}^{\dagger} + \frac{6i}{\omega_d} G_{3,S} e^{i\omega_d t/2} \hat{a}^{\dagger} \hat{a}^{\dagger} \hat{a} \\ - \frac{6i}{\omega_d} G_{3,S} e^{-i\omega_d t/2} \hat{a}^{\dagger} \hat{a} \hat{a} - \frac{2i}{3\omega_d} G_{3,S} e^{-3i\omega_d t/2} \hat{a} \hat{a} \hat{a}, \end{aligned} \quad (\text{A34})$$

where

$$\begin{aligned} \mathcal{G}_{31}(t) = \frac{i}{\hbar\omega_d^2} \left(\tilde{G}_{1,S} G_{2,S} \left(\frac{38}{25} e^{-5i\omega_d t/2} + \frac{71}{105} e^{7i\omega_d t/2} + \frac{46}{45} e^{3i\omega_d t/2} + \frac{19}{5} e^{-i\omega_d t/2} \right) \right. \\ \left. + G_{1,S} G_{2,S} \left(3e^{3i\omega_d t/2} - 2e^{-i\omega_d t/2} \right) + 6\hbar\omega_d G_{3,S} e^{i\omega_d t/2} \right). \end{aligned} \quad (\text{A35})$$

Since all the oscillating terms in $\hat{H}^{(i)}$ gets cancelled with the corresponding terms in $\partial_t \hat{S}^{(i)}$ and its commutators, Eqs. (A27) will be largely simplified. The resulting static Hamiltonian can be written as

$$\begin{aligned} \hat{\mathcal{H}}_{\text{st}} = \sum_{i=1}^4 \hat{\mathcal{H}}^{(i)} = \text{non osc} \left(\frac{1}{i\hbar} [\hat{S}^{(1)}, \hat{H}^{(1)}] + \frac{1}{2i\hbar} [\hat{S}^{(1)}, \partial_t \hat{S}^{(1)}] + \frac{1}{i\hbar} [\hat{S}^{(1)}, \hat{H}^{(2)}] \right. \\ \left. + \frac{1}{i\hbar} [\hat{S}^{(2)}, \hat{H}^{(1)}] + \frac{1}{2!(i\hbar)^2} [\hat{S}^{(1)}, [\hat{S}^{(1)}, \hat{H}^{(1)}]] + \frac{1}{2i\hbar} \left([S^{(1)}, \partial_t S^{(2)}] \right. \right. \\ \left. \left. + [S^{(2)}, \partial_t S^{(1)}] \right) + \frac{1}{3!(i\hbar)^2} [S^{(1)}, [S^{(1)}, \partial_t S^{(1)}]] + \mathcal{O}(\varphi_{zps}^4) \right), \end{aligned} \quad (\text{A36})$$

where non osc ($g(t)$) extracts the time-independent terms in $g(t)$. We find

$$\hat{\mathcal{H}}_{\text{st}} = \left(-\frac{2G_{2,S}^2}{\omega_d} - 2K \right) \hat{a}^{\dagger} \hat{a} \quad (\text{A37})$$

Hence, the static effective Hamiltonian up to $\mathcal{O}(\varphi_{zps}^4)$ is given by

$$\hat{\mathcal{H}}_S = \hat{H}_{\text{st}} + \hat{\mathcal{H}}_{\text{st}} = \Delta \hat{a}^{\dagger} \hat{a} + \epsilon_2 \left(\hat{a}^{\dagger 2} + \hat{a}^2 \right) - K \hat{a}^{\dagger 2} \hat{a}^2 + \Lambda \left(\hat{a}^{\dagger 3} \hat{a} + \hat{a}^3 \hat{a}^{\dagger} \right), \quad (\text{A38})$$

where $\Delta = \delta - \frac{2G_{2,S}^2}{\omega_d} - \frac{24G_{1,S}G_{3,S}}{\omega_d} - 2K$, $K = E_C/2$, $\epsilon_2 = G_{2,S} + 6G_{4,S}$ and $\Lambda = 4G_{4,S}$.

Appendix B: STS - Master Equation

In this section, we will study the dynamics of the STS in the presence of a thermal environment. The Kerr-cat Hamiltonian in Eq. (A38) acts as the system Hamiltonian. The system bath Hamiltonian in the rotating frame is given by

$$\hat{H}_{\text{SB}}(t) = i \left(\hat{a} e^{-i\omega_d t/2} - \hat{a}^{\dagger} e^{i\omega_d t/2} \right) \hat{B}(t), \quad (\text{B1})$$

where $\hat{B}(t) = \sum_j i h_j \left(\hat{b}_j e^{-i\omega_j t} - \hat{b}_j^\dagger e^{i\omega_j t} \right)$, \hat{b}_j (\hat{b}_j^\dagger) are the annihilation (creation) operators of mode j of the bosonic environment and h_j determines the system-bath coupling strength. The system-bath Hamiltonian, $\hat{H}_{\text{SB}}(t)$ is independent of the zero point spread of the phase operator ($\mathcal{O}(\varphi_{\text{zps}}^0)$). Similar to the case of system Hamiltonian, we do the generalized Schrieffer-Wolff transformation to the system-bath coupling Hamiltonian at various orders of zero point spread of the phase operator. We find

$$\begin{aligned}\hat{\mathcal{H}}_{\text{SB}}^{(0)} &= \hat{H}_{\text{SB}}, \\ \hat{\mathcal{H}}_{\text{SB}}^{(1)} &= \frac{1}{i\hbar} \left[\hat{S}^{(1)}, \hat{H}_{\text{SB}} \right], \\ \hat{\mathcal{H}}_{\text{SB}}^{(2)} &= \frac{1}{i\hbar} \left[\hat{S}^{(2)}, \hat{H}_{\text{SB}} \right] + \frac{1}{2!(i\hbar)^2} \left[\hat{S}^{(1)}, \left[\hat{S}^{(1)}, \hat{H}_{\text{SB}} \right] \right], \\ \hat{\mathcal{H}}_{\text{SB}}^{(3)} &= \frac{1}{i\hbar} \left[\hat{S}^{(3)}, \hat{H}_{\text{SB}} \right] + \frac{1}{2!(i\hbar)^2} \left(\left[\hat{S}^{(1)}, \left[\hat{S}^{(2)}, \hat{H}_{\text{SB}} \right] \right] + \left[\hat{S}^{(2)}, \left[\hat{S}^{(1)}, \hat{H}_{\text{SB}} \right] \right] \right) + \frac{1}{3!(i\hbar)^3} \left[\hat{S}^{(1)}, \left[\hat{S}^{(1)}, \left[\hat{S}^{(1)}, \hat{H}_{\text{SB}} \right] \right] \right].\end{aligned}\quad (\text{B2})$$

We dropped the time dependence of the generator and the Hamiltonian, for the sake of simplicity. Since, both $\hat{S}^{(1)}$ and \hat{H}_{SB} are linear in the annihilation and creation operators, $\hat{\mathcal{H}}_{\text{SB}}^{(1)}$ will be a scalar and would not contribute towards the system-bath dynamics. By the same reasoning, $\left[\hat{S}^{(1)}, \left[\hat{S}^{(1)}, \hat{H}_{\text{SB}} \right] \right] = 0$ and hence

$$\hat{\mathcal{H}}_{\text{SB}}^{(2)}(t) = \frac{\left[\hat{S}^{(2)}(t), \hat{H}_{\text{SB}}(t) \right]}{i\hbar}, \quad (\text{B3})$$

which simplifies to

$$\hat{\mathcal{H}}_{\text{SB}}^{(2)}(t) = \frac{iG_{2,S}}{\hbar\omega_d} \left\{ 3(-\hat{a}^\dagger e^{3i\omega_d t/2} + \hat{a} e^{-3i\omega_d t/2}) + 2(-\hat{a} e^{i\omega_d t/2} + \hat{a}^\dagger e^{-i\omega_d t/2}) \right\} \hat{B}(t). \quad (\text{B4})$$

The asymmetry in Josephson junction has no contribution on the bath induced dynamics of the system till $\mathcal{O}(\varphi_{\text{zps}}^2)$. Disregarding the scalars, the system-bath Hamiltonian at $\mathcal{O}(\varphi_{\text{zps}}^3)$ is given by

$$\hat{\mathcal{H}}_{\text{SB}}^{(3)}(t) = \frac{1}{i\hbar} \left[\hat{S}^{(3)}(t), \hat{H}_{\text{SB}}(t) \right], \quad (\text{B5})$$

which evaluates to

$$\mathcal{H}_{\text{SB}}^{(3)}(t) = \frac{8iG_{3,S}}{\hbar\omega_d} \left(e^{-i\omega_d t} \hat{a}^2 - e^{i\omega_d t} \hat{a}^{\dagger 2} \right). \quad (\text{B6})$$

Similarly, the fourth order contribution ($\mathcal{O}(\varphi_{\text{zps}}^4)$) can be simplified to

$$\hat{\mathcal{H}}_{\text{SB}}^{(4)}(t) = \frac{1}{i\hbar} \left[\hat{S}^{(4)}(t), \hat{H}_{\text{SB}}(t) \right] + \frac{1}{2!(i\hbar)^2} \left\{ \left[\hat{S}^{(2)}(t), \left[\hat{S}^{(2)}(t), \hat{H}_{\text{SB}}(t) \right] \right] + \left[\hat{S}^{(1)}(t), \left[\hat{S}^{(3)}(t), \hat{H}_{\text{SB}}(t) \right] \right] \right\}, \quad (\text{B7})$$

where the fourth order transformation is given as

$$\hat{S}^{(4)}(t) = - \int \text{osc} \left(\hat{H}^{(4)} + \frac{\left[\hat{S}^{(1)}, \hat{H}^{(3)} \right]}{i} + \frac{\left[\hat{S}^{(2)}, \hat{H}^{(2)} \right]}{i} + \frac{\left[\hat{S}^{(3)}, \hat{H}^{(1)} \right]}{i} + \frac{\left[\hat{S}^{(1)}, \partial_t \hat{S}^{(3)} \right]}{2i} + \frac{\left[\hat{S}^{(2)}, \partial_t \hat{S}^{(2)} \right]}{2i} + \frac{\left[\hat{S}^{(3)}, \partial_t \hat{S}^{(1)} \right]}{2i} \right) dt \quad (\text{B8})$$

After some calculations, we obtain

$$\begin{aligned}\hat{\mathcal{H}}_{\text{SB}}^{(4)}(t) &= i \left\{ \left(\frac{13G_{2,S}^2}{2\hbar^2\omega_d^2} \hat{a} - \frac{24G_{1,S}G_{3,S}}{\hbar^2\omega_d^2} \hat{a} + \frac{12G_{4,S}}{\hbar\omega_d} \hat{a}^\dagger + \frac{4G_{4,S}}{\hbar\omega_d} \hat{a}^3 + \frac{12G_{4,S}}{\hbar\omega_d} \hat{a}^{\dagger 2} \hat{a} \right) e^{-i\omega_d t/2} \right. \\ &\quad + \left(\frac{18G_{4,S}}{\hbar\omega_d} \hat{a} - \frac{11G_{2,S}^2}{\hbar^2\omega_d^2} \hat{a}^\dagger + \frac{12\tilde{G}_{1,S}G_{3,S}}{5\hbar^2\omega_d^2} \hat{a}^\dagger + \frac{12G_{4,S}}{\hbar\omega_d} \hat{a}^\dagger \hat{a}^2 \right) e^{-i3\omega_d t/2} \\ &\quad \left. + \left(\frac{13G_{2,S}^2}{3\hbar^2\omega_d^2} \hat{a} + \frac{4\tilde{G}_{1,S}G_{3,S}}{3\hbar^2\omega_d^2} \hat{a} + \frac{4G_{4,S}}{3\hbar\omega_d} \hat{a}^3 \right) e^{-i5\omega_d t/2} \right\} \hat{B}(t) + \text{h.c.}\end{aligned}\quad (\text{B9})$$

The total system-bath Hamiltonian

$$\hat{\mathcal{H}}_{\text{SB}}(t) = \sum_{k=0}^4 \hat{\mathcal{H}}_{\text{SB}}^{(k)}(t) \quad (\text{B10})$$

We start by writing the system-bath coupling Hamiltonian as

$$\hat{\mathcal{H}}_{\text{SB}}(t) = \sum_{\alpha=1}^n \hat{A}_{\alpha}(t) \otimes \hat{B}_{\alpha}(t), \quad (\text{B11})$$

where $\hat{B}_{\alpha}(t) = \hat{B}(t)$ for all α . In addition, we group the system operators such that $\hat{A}_{\alpha}(\tau) = \hat{A}_{\alpha}^{\dagger}(\tau)$ for the sake of simplification. We also define $\hat{A}_{\alpha} = \hat{A}_{\alpha}(\tau = 0)$. In the interaction picture, the system bath coupling Hamiltonian will read as

$$\hat{\mathcal{H}}_{\text{SB}}(t) = e^{\frac{i}{\hbar} \hat{\mathcal{H}}_{\text{S}} t} \hat{\mathcal{H}}_{\text{SB}}(t) e^{-\frac{i}{\hbar} \hat{\mathcal{H}}_{\text{S}} t} = \sum_{\alpha} e^{\frac{i}{\hbar} \mathcal{H}_{\text{S}} t} A_{\alpha} e^{-\frac{i}{\hbar} \mathcal{H}_{\text{S}} t} \otimes B_{\alpha}(t) = \sum_{\alpha} \tilde{A}_{\alpha}(t) \otimes \tilde{B}_{\alpha}(t), \quad (\text{B12})$$

where $\tilde{B}_{\alpha}(t) = B_{\alpha}(t)$. In the interaction picture, the Liouville equation for the density matrix can be written as

$$\frac{d\hat{\rho}(t)}{dt} = -\frac{i}{\hbar} \left[\hat{\mathcal{H}}_{\text{SB}}(t), \hat{\rho}(t) \right]. \quad (\text{B13})$$

Integrating above equation on both sides with respect to time, we obtain

$$\hat{\rho}(t) = -\frac{i}{\hbar} \int_0^t \left[\hat{\mathcal{H}}_{\text{SB}}(t'), \hat{\rho}(t') \right] dt' + \hat{\rho}(0) \quad (\text{B14})$$

Substituting Eq. (B14) in Eq. (B13), we obtain

$$\frac{d\hat{\rho}(t)}{dt} = -\frac{i}{\hbar} \left[\hat{\mathcal{H}}_{\text{SB}}(t), \hat{\rho}(0) \right] - \frac{1}{\hbar^2} \int_0^t \left[\hat{\mathcal{H}}_{\text{SB}}(t), \left[\hat{\mathcal{H}}_{\text{SB}}(t'), \hat{\rho}(t') \right] \right] dt'. \quad (\text{B15})$$

Tracing out the bath degrees of freedom from both sides of above equation, we get

$$\frac{d\hat{\rho}_{\text{S}}(t)}{dt} = -\frac{i}{\hbar} \text{Tr}_{\text{B}} \left[\hat{\mathcal{H}}_{\text{SB}}(t), \hat{\rho}(0) \right] - \frac{1}{\hbar^2} \text{Tr}_{\text{B}} \int_0^t \left[\hat{\mathcal{H}}_{\text{SB}}(t), \left[\hat{\mathcal{H}}_{\text{SB}}(t'), \hat{\rho}(t') \right] \right] dt'. \quad (\text{B16})$$

Born Approximation:

Considering macroscopic and bulky environment, we can assume that the bath dynamics is fast and there is no change to bath statistics due to system-bath coupling. Factorising the system and bath degrees of freedom in the density matrix, we have

$$\hat{\rho}(t) = \hat{\rho}_{\text{S}}(t) \otimes \hat{\rho}_{\text{B}}. \quad (\text{B17})$$

Eq. (B16) reduces to

$$\frac{d\hat{\rho}_{\text{S}}(t)}{dt} = -\frac{i}{\hbar} \text{Tr}_{\text{B}} \left[\hat{\mathcal{H}}_{\text{SB}}(t), \hat{\rho}_{\text{S}}(0) \otimes \hat{\rho}_{\text{B}} \right] - \frac{1}{\hbar^2} \int_0^t \left[\hat{\mathcal{H}}_{\text{SB}}(t), \left[\hat{\mathcal{H}}_{\text{SB}}(t'), \hat{\rho}_{\text{S}}(t') \otimes \hat{\rho}_{\text{B}} \right] \right] dt'. \quad (\text{B18})$$

Above equation is second order in $\hat{\mathcal{H}}_{\text{SB}}$ and all the higher order terms are neglected. This leads from the approximation in Eq. (B17) and is known as the Born approximation. The first term on the right hand side of above equation vanishes since

$$\text{Tr}_{\text{B}} \left[\hat{B}(t) \hat{\rho}_{\text{B}}(0) \right] = 0. \quad (\text{B19})$$

Using Eqs. (B12) and (B18), we obtain

$$\frac{d\hat{\rho}_{\text{S}}(t)}{dt} = -\frac{1}{\hbar^2} \sum_{\alpha, \beta} \int_0^t dt' \text{Tr}_{\text{B}} \left[\hat{A}_{\alpha}(t) \otimes \hat{B}_{\alpha}(t), \left[\hat{A}_{\beta}(t') \otimes \hat{B}_{\beta}(t'), \hat{\rho}_{\text{S}}(t') \otimes \hat{\rho}_{\text{B}} \right] \right] \quad (\text{B20})$$

Expanding the commutators, we obtain

$$\begin{aligned} \frac{d\hat{\rho}_S(t)}{dt} = & -\frac{1}{\hbar^2} \sum_{\alpha\beta} \int_0^t dt' \left[\hat{A}_\alpha(t) \hat{A}_\beta(t') \hat{\rho}_S(t') \text{Tr}_B \left[\hat{B}_\alpha(t) \hat{B}_\beta(t') \hat{\rho}_B \right] \right. \\ & - \hat{A}_\alpha(t) \hat{\rho}_S(t') \hat{A}_\beta(t') \text{Tr}_B \left[\hat{B}_\alpha(t) \hat{\rho}_B \hat{B}_\beta(t') \right] \\ & - \hat{A}_\beta(t') \hat{\rho}_S(t') \hat{A}_\alpha(t) \text{Tr}_B \left[\hat{B}_\beta(t') \hat{\rho}_B \hat{B}_\alpha(t) \right] \\ & \left. + \hat{\rho}_S(t') \hat{A}_\beta(t') \hat{A}_\alpha(t) \text{Tr}_B \left[\hat{\rho}_B \hat{B}_\beta(t') \hat{B}_\alpha(t) \right] \right]. \end{aligned} \quad (\text{B21})$$

Using the cyclic property of trace and organizing the bath operators, we obtain

$$\frac{d\hat{\rho}_S(t)}{dt} = -\frac{1}{\hbar^2} \sum_{\alpha\beta} \int_0^t dt' \left[C_{\alpha\beta}(t, t') \left[\hat{A}_\alpha(t), \hat{A}_\beta(t') \hat{\rho}_S(t') \right] + C_{\beta\alpha}(t', t) \left[\hat{\rho}_S(t') \hat{A}_\beta(t'), \hat{A}_\alpha(t) \right] \right], \quad (\text{B22})$$

where

$$C_{\alpha\beta}(t_1, t_2) = \text{Tr}_B \left[\hat{B}_\alpha(t_1) \hat{B}_\beta(t_2) \hat{\rho}_B \right]. \quad (\text{B23})$$

Markov Approximation:

Since, $[\hat{\mathcal{H}}_B, \hat{\rho}_B] = 0$, we have $C_{\alpha\beta}(t_1, t_2) = C_{\alpha\beta}(t_1 - t_2) = C_{\alpha\beta}(\tau)$, where $\tau = t_1 - t_2$. Further, assuming the bath operators in the contact Hamiltonian to be hermitian, i.e. $B_\alpha = B_\alpha^\dagger$, we have $C_{\alpha\beta}(\tau) = C_{\beta\alpha}^\dagger(-\tau)$. We will assume that the system density matrix varies very slowly compared to the decay time of the bath correlations. This assumption leads us to the first Markov approximation,

$$\frac{d\hat{\rho}_S(t)}{dt} = -\frac{1}{\hbar^2} \sum_{\alpha\beta} \int_0^t dt' \left[C_{\alpha\beta}(\tau) \left[\hat{A}_\alpha(t), \hat{A}_\beta(t') \hat{\rho}_S(t) \right] + C_{\beta\alpha}(-\tau) \left[\hat{\rho}_S(t) \hat{A}_\beta(t'), \hat{A}_\alpha(t) \right] \right], \quad (\text{B24})$$

where we replaced $\hat{\rho}_S(t')$ with $\hat{\rho}_S(t)$. Since, the bath correlation function decays rapidly, the integration limit can be extended to $t \rightarrow \infty$ without affecting the dynamics. We are only interested in the time far longer than the characteristic decay time of bath correlations. This is the second Markov approximation. Using the two Markov approximations the master equation is given by

$$\frac{d\hat{\rho}_S(t)}{dt} = -\frac{1}{\hbar^2} \sum_{\alpha\beta} \int_0^\infty d\tau \left[C_{\alpha\beta}(\tau) \left[\hat{A}_\alpha(t), \hat{A}_\beta(t-\tau) \hat{\rho}_S(t) \right] + C_{\beta\alpha}(-\tau) \left[\hat{\rho}_S(t) \hat{A}_\beta(t-\tau), \hat{A}_\alpha(t) \right] \right]. \quad (\text{B25})$$

Going back to the Schrödinger picture, we obtain

$$\frac{d\hat{\rho}_S(t)}{dt} = -\frac{i}{\hbar^2} \left[\hat{\mathcal{H}}_S, \hat{\rho}_S(t) \right] - \frac{1}{\hbar} \sum_{\alpha\beta} \int_0^\infty d\tau \left[C_{\alpha\beta}(\tau) \left[\hat{A}_\alpha, \hat{A}_\beta(-\tau) \hat{\rho}_S(t) \right] + C_{\beta\alpha}(-\tau) \left[\hat{\rho}_S(t) \hat{A}_\beta(-\tau), \hat{A}_\alpha \right] \right]. \quad (\text{B26})$$

Since $\hat{B}_\alpha(\tau) = \sum_j i h_j \left(\hat{b}_j e^{-i\omega_j \tau} - \hat{b}_j^\dagger e^{i\omega_j \tau} \right)$, $C_{\alpha\beta}(\tau)$ reduces to

$$C_{\alpha\beta}(\tau) = \text{Tr}_B \left[\hat{B}_\alpha(\tau) \hat{B}_\beta \rho_B \right] = \sum_j |h_j|^2 \left[e^{-i\omega_j \tau} (1 + n(\omega_j)) + e^{i\omega_j \tau} n(\omega_j) \right], \quad (\text{B27})$$

where $n(\omega_j) = \text{Tr}_B \left[\hat{b}_j^\dagger \hat{b}_j \rho_B \right]$ is the Bose-Einstein distribution function. Next, we will demonstrate the calculation of up to $(\mathcal{O}(\varphi_{zps}^2))$ master equation, i.e. for $\hat{\mathcal{H}}_{\text{SB}} = \hat{H}_{\text{SB}} + \hat{\mathcal{H}}_{\text{SB}}^{(2)}$. Note that, $\hat{\mathcal{H}}_{\text{SB}}^{(1)}$, which is the first order in φ_{zps} contribution, is a scalar and does not induce any dynamics. In this case, we have

$$\begin{aligned} \hat{A}_1(\tau) &= i \left(\hat{a} e^{-i\omega_d \tau/2} - \hat{a}^\dagger e^{i\omega_d \tau/2} \right), \\ \hat{A}_2(\tau) &= \frac{3iG_{2,S}}{\hbar\omega_d} \left(\hat{a} e^{-3i\omega_d \tau/2} - \hat{a}^\dagger e^{3i\omega_d \tau/2} \right), \\ \hat{A}_3(\tau) &= \frac{2iG_{2,S}}{\hbar\omega_d} \left(-\hat{a} e^{i\omega_d \tau/2} + \hat{a}^\dagger e^{-i\omega_d \tau/2} \right). \end{aligned} \quad (\text{B28})$$

The general form of \hat{A}_β can be written as

$$\hat{A}_\beta(\tau) = iA_\beta^{(0)}(\hat{X}_\beta e^{i\omega_\beta\tau} - \hat{X}_\beta^\dagger e^{-i\omega_\beta\tau}), \quad (\text{B29})$$

where $A_\beta^{(0)}$ is a constant. This rewriting of the system operator will hugely simplify the calculation later when we encounter multi-photon effects while considering $\hat{\mathcal{H}}_{\text{SB}}^{(3)}$ and $\hat{\mathcal{H}}_{\text{SB}}^{(4)}$.

The general expression for the integrals in Eq. (B26) can then be written as

$$\begin{aligned} I_{+\beta} = \frac{1}{\hbar^2} \int_0^\infty C_{\alpha\beta}(\tau) \hat{A}_\beta(-\tau) d\tau = \frac{iA_\beta^{(0)}}{2\hbar^2} \left\{ n'(\omega_j) \hat{X}_\beta \left[2\pi \sum_j |h_j|^2 \delta(-\omega_\beta - \omega_j) \right] - n'(\omega_j) \hat{X}_\beta^\dagger \left[2\pi \sum_j |h_j|^2 \delta(\omega_\beta - \omega_j) \right] \right. \\ \left. + n(\omega_j) \hat{X}_\beta \left[2\pi \sum_j |h_j|^2 \delta(\omega_j - \omega_\beta) \right] - n(\omega_j) \hat{X}_\beta^\dagger \left[2\pi \sum_j |h_j|^2 \delta(\omega_\beta + \omega_j) \right] \right\}, \quad (\text{B30}) \end{aligned}$$

where $n'(\omega_j) = (1 + n(\omega_j))$. Similarly,

$$\begin{aligned} I_{-\beta} = \frac{1}{\hbar^2} \int_0^\infty C_{\alpha\beta}(-\tau) \hat{A}_\beta(-\tau) d\tau = \frac{iA_\beta^{(0)}}{2\hbar^2} \left\{ n'(\omega_j) X_\beta \left[2\pi \sum_j |h_j|^2 \delta(\omega_j - \omega_\beta) \right] - n'(\omega_j) X_\beta^\dagger \left[2\pi \sum_j |h_j|^2 \delta(\omega_\beta + \omega_j) \right] \right. \\ \left. + n(\omega_j) X_\beta \left[2\pi \sum_j |h_j|^2 \delta(-\omega_j - \omega_\beta) \right] - n(\omega_j) X_\beta^\dagger \left[2\pi \sum_j |h_j|^2 \delta(\omega_\beta - \omega_j) \right] \right\} \quad (\text{B31}) \end{aligned}$$

Defining the spectral density of the bath as

$$\kappa(\omega) = \frac{2\pi}{\hbar} \sum_j |h_j|^2 \delta(\omega_j - \omega), \quad (\text{B32})$$

we obtain

$$\begin{aligned} \hat{I}_{+\beta} &= \frac{iA_\beta^{(0)} \hat{X}_\beta}{2\hbar} (n(\omega_\beta)\kappa(\omega_\beta) + n'(-\omega_\beta)\kappa(-\omega_\beta)) - \frac{iA_\beta^{(0)} \hat{X}_\beta^\dagger}{2\hbar} (n'(\omega_\beta)\kappa(\omega_\beta) + n(-\omega_\beta)\kappa(-\omega_\beta)), \\ \hat{I}_{-\beta} &= \frac{iA_\beta^{(0)} \hat{X}_\beta}{2\hbar} (n'(\omega_\beta)\kappa(\omega_\beta) + n(-\omega_\beta)\kappa(-\omega_\beta)) - \frac{iA_\beta^{(0)} \hat{X}_\beta^\dagger}{2\hbar} (n'(-\omega_\beta)\kappa(-\omega_\beta) + n(\omega_\beta)\kappa(\omega_\beta)). \quad (\text{B33}) \end{aligned}$$

Using above equations, Eq. (B26) reduces to

$$\frac{d\hat{\rho}_S(t)}{dt} = -\frac{i}{\hbar} [\hat{\mathcal{H}}_S, \hat{\rho}_S(t)] - \sum_{\alpha\beta} \left([\hat{A}_\alpha, \hat{I}_{+\beta} \hat{\rho}_S(t)] + [\hat{\rho}_S(t) \hat{I}_{-\beta}, \hat{A}_\alpha] \right). \quad (\text{B34})$$

Let us consider one of the possible cases, $\alpha = \beta = 1$, such that $A_\alpha = A_1 = i(\hat{a} - \hat{a}^\dagger)$, $A_\beta^{(0)} = 1$, $X_\beta = -\hat{a}^\dagger$, $X_\beta^\dagger = -\hat{a}$, and $\omega_\beta = \frac{\omega_d}{2}$. We find

$$\hat{I}_{\pm 1} = \frac{-i\hat{a}^\dagger}{2} \gamma(\pm\omega_d/2) + \frac{i\hat{a}}{2} \gamma(\mp\omega_d/2), \quad (\text{B35})$$

where we defined the transition rate as $\gamma(\omega) = \kappa(\omega)n(\omega)/\hbar$. Similarly, we can calculate the integrals $\hat{I}_{\pm\beta}$ for all β and substitute it in Eq. (B34). After some calculations, we obtain

$$\begin{aligned} \frac{d\hat{\rho}_S}{dt} = \frac{-i}{\hbar} [\mathcal{H}_S, \hat{\rho}_S(t)] + \frac{1}{\hbar} \kappa(\omega_d/2) \left\{ n(\omega_d/2) \mathcal{D} \left[a^\dagger + \frac{2G_{2,S}}{\hbar\omega_d} a \right] \hat{\rho}_S(t) + [n(\omega_d/2) + 1] \mathcal{D} \left[a + \frac{2G_{2,S}}{\hbar\omega_d} a^\dagger \right] \hat{\rho}_S(t) \right\} \\ + \frac{1}{\hbar} \left(\frac{3G_{2,S}}{\hbar\omega_d} \right)^2 \kappa(3\omega_d/2) \left\{ n(3\omega_d/2) \mathcal{D} [a^\dagger] \hat{\rho}_S(t) + [n(3\omega_d/2) + 1] \mathcal{D} [a] \hat{\rho}_S(t) \right\}. \quad (\text{B36}) \end{aligned}$$

The above master equation is $\mathcal{O}(\varphi_{\text{zps}}^2)$. In order to go beyond second order in φ_{zps} , we will consider the higher order contribution to the system-bath coupling Hamiltonian. Taking $\hat{\mathcal{H}}_{\text{SB}}^{(3)}$ and $\hat{\mathcal{H}}_{\text{SB}}^{(4)}$, we obtain the effective Lindblad master equation given by

$$\begin{aligned}
\frac{d\hat{\rho}_{\text{S}}^{3,4}}{dt} = & \frac{1}{\hbar}\kappa(\omega_d)\left\{n(\omega_d)\mathcal{D}\left[\frac{8G_{3,S}}{\hbar\omega_d}\hat{a}^\dagger\right]\hat{\rho}_{\text{S}}(t) + [n(\omega_d) + 1]\mathcal{D}\left[\frac{8G_{3,S}}{\hbar\omega_d}\hat{a}^2\right]\hat{\rho}_{\text{S}}(t)\right\} \\
& + \frac{1}{\hbar}\kappa(\omega_d/2)\left\{n(\omega_d/2)\mathcal{D}\left[\frac{3G_{2,S}^2}{2\hbar^2\omega_d^2}\hat{a}^\dagger - \frac{24G_{1,S}G_{3,S}}{\hbar^2\omega_d^2}\hat{a}^\dagger + \frac{12G_{4,S}}{\hbar\omega_d}\hat{a} + \frac{4G_{4,S}}{\hbar\omega_d}\hat{a}^{\dagger 3} + \frac{12G_{4,S}}{\hbar\omega_d}\hat{a}^\dagger\hat{a}^2\right]\hat{\rho}_{\text{S}}(t)\right. \\
& \left. + [n(\omega_d/2) + 1]\mathcal{D}\left[\frac{3G_{2,S}^2}{2\hbar^2\omega_d^2}\hat{a} - \frac{24G_{1,S}G_{3,S}}{\hbar^2\omega_d^2}\hat{a} + \frac{12G_{4,S}}{\hbar\omega_d}\hat{a}^\dagger + \frac{4G_{4,S}}{\hbar\omega_d}\hat{a}^3 + \frac{12G_{4,S}}{\hbar\omega_d}\hat{a}^{\dagger 2}\hat{a}\right]\hat{\rho}_{\text{S}}(t)\right\} \\
& + \frac{1}{\hbar}\kappa(3\omega_d/2)\left\{n(3\omega_d/2)\mathcal{D}\left[\frac{18G_{4,S}}{\hbar\omega_d}\hat{a}^\dagger - \frac{11G_{2,S}^2}{\hbar^2\omega_d^2}\hat{a} + \frac{12\tilde{G}_{1,S}G_{3,S}}{5\hbar^2\omega_d^2}\hat{a} + \frac{12G_{4,S}}{\hbar\omega_d}\hat{a}^{\dagger 2}\hat{a}\right]\hat{\rho}_{\text{S}}(t)\right. \\
& \left. + [n(3\omega_d/2) + 1]\mathcal{D}\left[\frac{18G_{4,S}}{\hbar\omega_d}\hat{a} - \frac{11G_{2,S}^2}{\hbar^2\omega_d^2}\hat{a}^\dagger + \frac{12\tilde{G}_{1,S}G_{3,S}}{5\hbar^2\omega_d^2}\hat{a}^\dagger + \frac{12G_{4,S}}{\hbar\omega_d}\hat{a}^\dagger\hat{a}^2\right]\hat{\rho}_{\text{S}}(t)\right\} \\
& + \frac{1}{\hbar}\kappa(5\omega_d/2)\left\{n(5\omega_d/2)\mathcal{D}\left[\frac{5G_{2,S}^2}{3\hbar^2\omega_d^2}\hat{a}^\dagger + \frac{4\tilde{G}_{1,S}G_{3,S}}{3\hbar^2\omega_d^2}\hat{a}^\dagger + \frac{4G_{4,S}}{3\hbar\omega_d}\hat{a}^{\dagger 3}\right]\hat{\rho}_{\text{S}}(t)\right. \\
& \left. + [n(5\omega_d/2) + 1]\mathcal{D}\left[\frac{5G_{2,S}^2}{3\hbar^2\omega_d^2}\hat{a} + \frac{4\tilde{G}_{1,S}G_{3,S}}{3\hbar^2\omega_d^2}\hat{a} + \frac{4G_{4,S}}{3\hbar\omega_d}\hat{a}^3\right]\hat{\rho}_{\text{S}}(t)\right\}, \quad (\text{B37})
\end{aligned}$$

where the terms in the first line are $\mathcal{O}(\varphi_{\text{zps}}^3)$ whereas the latter terms are $\mathcal{O}(\varphi_{\text{zps}}^4)$.

1. Single photon processes and RWA

The master equation in the RWA can be written as

$$\partial_t \hat{\rho}_{\text{S}} = \hat{\mathcal{L}}\hat{\rho}_{\text{S}} = -\frac{i}{\hbar}\left[\hat{\mathcal{H}}_{\text{S}}, \hat{\rho}_{\text{S}}\right] + \frac{1}{\hbar}\kappa n(\omega_d/2)\mathcal{D}[\hat{a}^\dagger]\hat{\rho}_{\text{S}} + \frac{1}{\hbar}\kappa(1 + n(\omega_d/2))\mathcal{D}[\hat{a}]\hat{\rho}_{\text{S}}, \quad (\text{B38})$$

where $\hat{\mathcal{L}}$ is the Liouvillian. We consider the spectral function to be energy independent such that $\kappa(\omega_d/2) = \kappa$. First we will calculate the eigenstates and eigenvectors of $\hat{\mathcal{H}}_{\text{S}}$,

$$\hat{\mathcal{H}}_{\text{S}}|\psi_m^\pm\rangle = \omega_m^\pm|\psi_m^\pm\rangle. \quad (\text{B39})$$

The lowest energy eigenstates of the Hamiltonian are given by the degenerate cat state manifold $\psi_0^\pm = \mathcal{C}_\alpha^\pm$. The lowest eigenvalue of the Liouvillian (λ) will give the coherence life time of the qubit, $T_X = [-\text{Re}\lambda]^{-1}$. The Liouvillian can be calculated from the master equation,

$$\hat{\mathcal{L}}\cdot = -\frac{i}{\hbar}\left[\hat{\mathcal{H}}_{\text{S}}, \cdot\right] + \frac{1}{\hbar}\kappa n(\omega_d/2)\mathcal{D}[\hat{a}^\dagger]\cdot + \frac{1}{\hbar}\kappa(1 + n(\omega_d/2))\mathcal{D}[\hat{a}]\cdot. \quad (\text{B40})$$

Following Ref. [13], we separate out the population and coherence subspace, we have

$$\begin{aligned}
\hat{\mathcal{B}}_{\text{pop}} &= \{|\psi_m^+\rangle\langle\psi_m^+|, |\psi_m^+\rangle\langle\psi_m^+|, \dots\} \quad \text{for } m \geq 0, \\
\hat{\mathcal{B}}_{\text{coh}} &= \{|\psi_m^+\rangle\langle\psi_m^-|, |\psi_m^-\rangle\langle\psi_m^+|, \dots\} \quad \text{for } m \geq 0.
\end{aligned} \quad (\text{B41})$$

We do not need to consider all m , since the higher lying states have smaller probabilities of getting populated. For example, for $\epsilon_2 = 0$, all the states with $\omega_n^+ - \omega_n^- > \kappa$ are beyond the reach of being excited.

Furthermore, we observe that under single photon loss and gain, the master equation corresponding to population and coherence are decoupled. Hence, we can study the decoherence mechanism separately from the population. In addition, the change in ρ_{S} is induced by the change in coherent state, the population states describe the steady state of the Lindbladian. The density matrix vector takes the following form

$$[\rho_{\text{S},0}^\pm \ \rho_{\text{S},1}^\pm \ \rho_{\text{S},2}^\pm \ \dots \ \rho_{\text{S},0}^\mp \ \rho_{\text{S},1}^\mp \ \rho_{\text{S},2}^\mp \ \dots]^T, \quad (\text{B42})$$

where $\rho_{S,m}^{\pm} = \langle \psi_m^+ | \hat{\rho}_S | \psi_m^- \rangle$. The corresponding Liouvillian superoperator is given by

$$\hat{\mathbf{L}} = \hat{\mathbf{L}}_H + \hat{\mathbf{L}}_D, \quad (\text{B43})$$

where $H(D)$ determined the unitary (dissipative) part of the Liouvillian. First of all, let's calculate the unitary part

$$-i \langle \psi_m^+ | [\hat{\mathcal{H}}_S, \hat{\rho}_S] | \psi_m^- \rangle = -i (\omega_m^+ - \omega_m^-) \rho_{S,m}^{\pm} = -i \delta_m \rho_{S,m}^{\pm}, \quad (\text{B44})$$

where $\delta_m = \omega_m^+ - \omega_m^-$. Note that, $\omega_0^+ - \omega_0^- = \delta_0 = 0$. Hence, in the block diagonal form,

$$\hat{\mathbf{L}}_H = \begin{bmatrix} -\Delta & 0 \\ 0 & \Delta \end{bmatrix}, \quad (\text{B45})$$

where

$$\Delta = \begin{bmatrix} 0 & & & \\ & i\delta_1 & & \\ & & i\delta_2 & \\ & & & \ddots \end{bmatrix}. \quad (\text{B46})$$

To calculate $\hat{\mathbf{L}}_D$, we first calculate $\langle \psi_m^+ | \mathcal{D}[\hat{O}] \hat{\rho}_S | \psi_m^- \rangle$ for a general operator \hat{O} . We can write $\hat{\rho}_S$ in the $\hat{\mathcal{B}}_{\text{coh}}$ basis and rewrite above expression as

$$\begin{aligned} \langle \psi_m^+ | \mathcal{D}[\hat{O}] \hat{\rho}_S | \psi_m^- \rangle &= \langle \psi_m^+ | \hat{O} \left(\sum_{\alpha\beta,i} \rho_{S,i}^{\alpha\beta} |\psi_i^\alpha\rangle \langle \psi_i^\beta| \right) \hat{O}^\dagger | \psi_m^- \rangle \\ &\quad - \frac{1}{2} \langle \psi_m^+ | \left[\hat{O}^\dagger \hat{O} \left(\sum_{\alpha\beta,i} \rho_{S,i}^{\alpha\beta} |\psi_i^\alpha\rangle \langle \psi_i^\beta| \right) + \left(\sum_{\alpha\beta,i} \rho_{S,i}^{\alpha\beta} |\psi_i^\alpha\rangle \langle \psi_i^\beta| \right) \hat{O}^\dagger \hat{O} \right] | \psi_m^- \rangle, \end{aligned} \quad (\text{B47})$$

where $\alpha, \beta = +, -$. With further simplification, the above equation reduces to

$$\langle \psi_m^+ | \mathcal{D}[\hat{O}] \hat{\rho}_S | \psi_m^- \rangle = \sum_{\alpha\beta,i} \langle \psi_m^+ | \hat{O} |\psi_i^\alpha\rangle \langle \psi_i^\beta | \hat{O}^\dagger | \psi_m^- \rangle \rho_{S,i}^{\alpha\beta} - \frac{1}{2} \left[\sum_{\alpha} \langle \psi_m^+ | \hat{O}^\dagger \hat{O} |\psi_m^\alpha\rangle \rho_{S,m}^{\alpha-} + \sum_{\beta} \langle \psi_m^\beta | \hat{O}^\dagger \hat{O} | \psi_m^- \rangle \rho_{S,m}^{+\beta} \right]. \quad (\text{B48})$$

The α in the second summation can only be $+$ and the β in the third summation can only be $-$, so the second and third summations can be dropped and we obtain

$$\langle \psi_m^+ | \mathcal{D}[\hat{O}] \hat{\rho}_S | \psi_m^- \rangle = \sum_{\alpha\beta,i} \langle \psi_m^+ | \hat{O} |\psi_i^\alpha\rangle \langle \psi_i^\beta | \hat{O}^\dagger | \psi_m^- \rangle \rho_{S,i}^{\alpha\beta} - \frac{1}{2} \left[\langle \psi_m^+ | \hat{O}^\dagger \hat{O} | \psi_m^+ \rangle + \langle \psi_m^- | \hat{O}^\dagger \hat{O} | \psi_m^- \rangle \right] \rho_{S,m}^{\pm}. \quad (\text{B49})$$

Substituting Eq. (B49) into Eq. (B40), we can rewrite the dissipative part of the Liouvillian superoperator in the matrix form as

$$\hat{\mathbf{L}}_D = \kappa(1 + n(\omega_d/2)) \begin{bmatrix} -\mathbf{A} & \mathbf{B} \\ \mathbf{B} & -\mathbf{A} \end{bmatrix} + \kappa n(\omega_d) \begin{bmatrix} -\mathbf{C} & \mathbf{D} \\ \mathbf{D} & -\mathbf{C} \end{bmatrix}, \quad (\text{B50})$$

where the block matrices $\mathbf{A}, \mathbf{B}, \mathbf{C}, \mathbf{D}$ are given by

$$\mathbf{A} = \begin{bmatrix} A_0 & & & \\ & A_1 & & \\ & & A_2 & \\ & & & \ddots \end{bmatrix}, \mathbf{B} = \begin{bmatrix} B_{00} & B_{01} & B_{02} \\ B_{10} & B_{11} & B_{12} \\ B_{20} & B_{21} & B_{22} \\ & & & \ddots \end{bmatrix}, \mathbf{C} = \begin{bmatrix} C_0 & & & \\ & C_1 & & \\ & & C_2 & \\ & & & \ddots \end{bmatrix}, \mathbf{D} = \begin{bmatrix} D_{00} & D_{01} & D_{02} \\ D_{10} & D_{11} & D_{12} \\ D_{20} & D_{21} & D_{22} \\ & & & \ddots \end{bmatrix}, \quad (\text{B51})$$

where the entries for each matrices are given by

$$A_m = \frac{1}{2} \left[\langle \psi_m^+ | \hat{O}^\dagger \hat{O} | \psi_m^+ \rangle + \langle \psi_m^- | \hat{O}^\dagger \hat{O} | \psi_m^- \rangle \right], \quad B_{mp} = \langle \psi_m^- | \hat{O} | \psi_p^+ \rangle \langle \psi_p^- | \hat{O}^\dagger | \psi_m^+ \rangle, \quad (\text{B52})$$

and

$$C_m = \frac{1}{2} \left[\langle \psi_m^+ | \hat{O} \hat{O}^\dagger | \psi_m^+ \rangle + \langle \psi_m^- | \hat{O} \hat{O}^\dagger | \psi_m^- \rangle \right], \quad D_{mp} = \langle \psi_m^- | \hat{O}^\dagger | \psi_p^+ \rangle \langle \psi_p^- | \hat{O} | \psi_m^+ \rangle. \quad (\text{B53})$$

2. Beyond RWA and multi-photon processes

The Liouvillian that we want to calculate is for the master equation up to φ_{zps}^3 which includes multi-photon effects

$$\begin{aligned} \frac{\partial \rho_S}{\partial t} = & -\frac{i}{\hbar} [\mathcal{H}_S, \rho_S(t)] + \frac{1}{\hbar} \kappa(\omega_d/2) \left\{ n(\omega_d/2) \mathcal{D} \left[\hat{a}^\dagger + \frac{2G_{2,S}}{\hbar\omega_d} \hat{a} \right] \hat{\rho}_S + [1 + n(\omega_d/2)] \mathcal{D} \left[\hat{a} + \frac{2G_{2,S}}{\hbar\omega_d} \hat{a}^\dagger \right] \hat{\rho}_S \right\} \\ & + \frac{1}{\hbar} \left(\frac{3G_{2,S}}{\hbar\omega_d} \right)^2 \kappa(3\omega_d/2) \left\{ n(3\omega_d/2) \mathcal{D} [a^\dagger] \hat{\rho}_S + [1 + n(3\omega_d/2)] \mathcal{D} [\hat{a}] \hat{\rho}_S \right\} \\ & + \frac{1}{\hbar} \left(\frac{8G_{3,S}}{\hbar\omega_d} \right)^2 \kappa(\omega_d) \left\{ n(\omega_d) \mathcal{D} [\hat{a}^{\dagger 2}] \hat{\rho}_S + [1 + n(\omega_d)] \mathcal{D} [\hat{a}^2] \hat{\rho}_S \right\}. \end{aligned} \quad (\text{B54})$$

The Liouvillian for the unitary part is the same as in the single photon case. The effective Liouvillian for the decoherence part is

$$\hat{\mathbf{L}}_{\text{eff}} = \hat{\mathbf{L}}_H + \hat{\mathbf{L}}_{D1} + \hat{\mathbf{L}}_{D2} + \hat{\mathbf{L}}_{D3} \quad (\text{B55})$$

where

$$\hat{\mathbf{L}}_{Di} = \frac{1}{\hbar} \kappa(\omega_i) (1 + n(\omega_i)) \begin{bmatrix} -\mathbf{A}^{Di} & \mathbf{B}^{Di} \\ \mathbf{B}^{Di} & -\mathbf{A}^{Di} \end{bmatrix} + \frac{1}{\hbar} \kappa(\omega_i) n(\omega_i) \begin{bmatrix} -\mathbf{C}^{Di} & \mathbf{D}^{Di} \\ \mathbf{D}^{Di} & -\mathbf{C}^{Di} \end{bmatrix}. \quad (\text{B56})$$

In above equation, we defined $\omega_1 = \omega_d/2$, $\omega_2 = 3\omega_d/2$ and $\omega_3 = \omega_d$. The matrix elements of the matrices \mathbf{A} , \mathbf{B} , \mathbf{C} and \mathbf{D} are given by Eqs. (B52) and (B53) by suitably replacing the operator \hat{O} by the corresponding single photon or multi-photon annihilation and creation operator. For instance, in the case of $\hat{\mathbf{L}}_{D3}$, $\hat{O} = \left(\frac{G_{3,S}}{8\hbar\omega_d} \right)^2 \hat{a}^2$ for the matrices \mathbf{A} and \mathbf{B} , and $\hat{O} = \left(\frac{G_{3,S}}{8\hbar\omega_d} \right)^2 \hat{a}^{\dagger 2}$ for the matrices \mathbf{C} and \mathbf{D} .

3. Effect of stronger modulation depth

In this section, we will study the effect of higher order terms in modulation depth to the master equation of STS taking symmetric junctions. If we have a stronger modulation depth, we must further expand $\sin(\delta\varphi \cos(\omega_d t))$ to third order, giving us a modulation depth of

$$\sin(\delta\varphi \cos(\omega_d t)) \approx \delta\varphi \cos(\omega_d t) - \frac{1}{3!} [\delta\varphi \cos(\omega_d t)]^3. \quad (\text{B57})$$

This modifies the Hamiltonian in Eq. (A4) to

$$\hat{H}_{\text{lab}} = 4E_C \hat{n}^2 - E_{J2} \cos \hat{\varphi} - 2E_{J\Sigma} \left[\delta\varphi \cos(\omega_d t) - \frac{1}{3!} [\delta\varphi \cos(\omega_d t)]^3 \right] \cos \hat{\varphi}, \quad (\text{B58})$$

where we assumed $E_{J\Delta} = 0$. We write $\cos(\omega_d t)$ in terms of exponential and Taylor expand $\cos \hat{\varphi}$ to fourth order to obtain

$$\hat{H}_{\text{lab}} = 4E_C \hat{n}^2 - E_{J2} \cos \hat{\varphi} - 2E_{J\Sigma} \left[\frac{\delta\varphi}{2} (e^{i\omega_d t} + e^{-i\omega_d t}) - \frac{\delta\varphi^3}{48} (e^{3i\omega_d t} + 3e^{i\omega_d t} + 3e^{-i\omega_d t} + e^{-3i\omega_d t}) \right] \left(1 - \frac{\hat{\varphi}^2}{2!} + \frac{\hat{\varphi}^4}{4!} \right). \quad (\text{B59})$$

If we write $\hat{\varphi}$ in terms of annihilation and creation operators as well as drop all scalars, we will get the Hamiltonian

$$\hat{H}_{\text{lab}} = \epsilon_c \hat{a}^\dagger \hat{a} - K \hat{a}^{\dagger 2} \hat{a}^2 + 2E_{J\Sigma} \left[\left(\frac{\delta\varphi}{2} - \frac{\delta\varphi^3}{16} \right) (e^{i\omega_d t} + e^{-i\omega_d t}) - \frac{\delta\varphi^3}{48} (e^{3i\omega_d t} + e^{-3i\omega_d t}) \right] \left[\frac{\varphi_{zps}^2}{2!} (\hat{a}^\dagger + \hat{a})^2 - \frac{\varphi_{zps}^4}{4!} (\hat{a}^\dagger + \hat{a})^4 \right]. \quad (\text{B60})$$

Now if we move to the rotating frame using $\hat{a} \rightarrow \hat{a} e^{-i\omega_d t/2}$ and rearrange some terms, we obtain

$$\hat{H}_T = \delta \hat{a}^\dagger \hat{a} - K \hat{a}^{\dagger 2} \hat{a}^2, \quad (\text{B61})$$

and

$$\hat{H}_{\text{SQ}}^{\text{sym}} = 2E_{\text{J}\Sigma} \left[\left(\frac{\delta\varphi}{2} - \frac{\delta\varphi^3}{16} \right) (e^{i\omega_d t} + e^{-i\omega_d t}) - \frac{\delta\varphi^3}{48} (e^{3i\omega_d t} + e^{-3i\omega_d t}) \right] \\ \left[\frac{\varphi_{\text{zps}}^2}{2!} (a^\dagger e^{i\omega_d t/2} + a e^{-i\omega_d t/2})^2 - \frac{\varphi_{\text{zps}}^4}{4!} (a^\dagger e^{i\omega_d t/2} + a e^{-i\omega_d t/2})^4 \right] \quad (\text{B62})$$

for the transmon and symmetric SQUID Hamiltonian, respectively. Following Appendix A 2, we perform the generalized Schrieffer-Wolff transformation and obtain the following static effective Hamiltonian

$$\mathcal{H}_S = \Delta \hat{a}^\dagger \hat{a} + (G_{2,S} - G'_{2,S} + 6G_{4,S} - 6G'_{4,S}) (\hat{a}^{\dagger 2} + \hat{a}^2) - K \hat{a}^{\dagger 2} \hat{a}^2 + 4(G_{4,S} - G'_{4,S}) (\hat{a}^\dagger \hat{a}^3 + \hat{a}^{\dagger 3} \hat{a}) \quad (\text{B63})$$

where $G_{2,S} = \frac{\delta\varphi E_{\text{J}\Sigma} \varphi_{\text{zps}}^2}{2}$, $G'_{2,S} = \frac{\delta\varphi^3 E_{\text{J}\Sigma} \varphi_{\text{zps}}^2}{16}$, $G_{4,S} = -\frac{\varphi_{\text{zps}}^2}{12} G_{2,S}$, $G'_{4,S} = \frac{\varphi_{\text{zps}}^2}{12} G'_{2,S}$, and the detuning, $\Delta = \delta - \frac{2(G_{2,S} - G'_{2,S})^2}{\omega_d} + \frac{G'_{2,S}}{9\omega_d}$. Similarly, the static effective interaction Hamiltonian is given by

$$\hat{\mathcal{H}}_{\text{SB}} = \frac{E_{\text{J}\Sigma} \varphi_{\text{zps}}^2}{i\omega_d} \left[\frac{3}{2} \left(\delta\varphi - \frac{\delta\varphi^3}{8} \right) (\hat{a}^\dagger e^{i3\omega_d t/2} - \hat{a} e^{-i3\omega_d t/2}) + \frac{5\delta\varphi^3}{144} (\hat{a}^\dagger e^{-i5\omega_d t/2} - \hat{a} e^{i5\omega_d t/2}) \right. \\ \left. + \frac{11\delta\varphi^3}{576} (\hat{a} e^{-i7\omega_d t/2} - \hat{a}^\dagger e^{i7\omega_d t/2}) + \left(\delta\varphi - \frac{\delta\varphi^3}{8} \right) (\hat{a} e^{i\omega_d t/2} - \hat{a}^\dagger e^{-i\omega_d t/2}) \right] \hat{B}(t). \quad (\text{B64})$$

Finally, the master equation up to order φ_{zps}^2 is given by

$$\partial_t \hat{\rho}_S(t) = \frac{1}{\hbar} \kappa(\omega_d/2) \left\{ n(\omega_d/2) \mathcal{D} \left[\hat{a}^\dagger + \frac{2(G_{2,S} - G'_{2,S})}{\hbar\omega_d} \hat{a} \right] \rho_S(t) + [n(\omega_d/2) + 1] \mathcal{D} \left[\hat{a} + \frac{2(G_{2,S} - G'_{2,S})}{\hbar\omega_d} \hat{a}^\dagger \right] \rho_S(t) \right\} \\ + \frac{1}{\hbar} \left[\frac{3(G_{2,S} - G'_{2,S})}{\hbar\omega_d} \right]^2 \kappa(3\omega_d/2) \left\{ n(3\omega_d/2) \mathcal{D}[\hat{a}^\dagger] \hat{\rho}_S(t) + [n(3\omega_d/2) + 1] \mathcal{D}[\hat{a}] \rho_S(t) \right\} \\ + \frac{1}{\hbar} \left(\frac{5G'_{2,S}}{8\hbar\omega_d} \right)^2 \kappa(5\omega_d/2) \left\{ n(5\omega_d/2) \mathcal{D}[\hat{a}] \rho_S(t) + [n(5\omega_d/2) + 1] \mathcal{D}[\hat{a}^\dagger] \hat{\rho}_S(t) \right\} \\ + \frac{1}{\hbar} \left(\frac{11G'_{2,S}}{36\hbar\omega_d} \right)^2 \kappa(7\omega_d/2) \left\{ n(7\omega_d/2) \mathcal{D}[\hat{a}^\dagger] \hat{\rho}_S(t) + [n(7\omega_d/2) + 1] \mathcal{D}[\hat{a}] \rho_S(t) \right\} - \frac{i}{\hbar} [\hat{\mathcal{H}}_S, \hat{\rho}_S(t)]. \quad (\text{B65})$$

Appendix C: SQUID Kerr-cat qubit - Hamiltonian and master equation

In this section, we will study the effective Hamiltonian and effective master equation for a driven SQUID and compare it to the case of STS. The Hamiltonian for a SQUID with symmetric junctions is given by (see Eq. (A3))

$$\hat{H}_{\text{lab,SQ}} = 4E_C \hat{n}^2 - 2E_{\text{J}\Sigma} \cos \hat{\varphi} \cos \tilde{\varphi}_e, \quad (\text{C1})$$

where $\tilde{\varphi}_e = \phi_e/2$ with $2\pi\phi_e/\phi_0$ being the external flux threading the SQUID. The charging energy is $E_C = e^2/2C$, where C is the total self-capacitance of the constituent Josephson junctions. We observe that for $\tilde{\varphi}_e = \pi/2$, $\hat{H}_{\text{lab,SQ}} = 4E_C \hat{n}^2$. This implies that the circuit becomes purely capacitive, and hence can't be operated as an oscillator around $\tilde{\varphi}_e = \pi/2$. However, a STS acts as a non-linear oscillator for $\varphi_\Sigma = \pi/2$ (see Eq. (A3)) and hence can be operated around $\varphi_\Sigma = \pi/2$. The SQUID can however be operated around $\tilde{\varphi}_e = \pi/4$. Let us consider

$$\tilde{\varphi}_e = \pi/4 + \delta\phi \cos(\omega_d t). \quad (\text{C2})$$

Inserting Eq. (C2) in Eq. (C1), we obtain

$$\hat{H}_{\text{lab,SQ}} = 4E_C \hat{n}^2 - \sqrt{2} E_{\text{J}\Sigma} (1 - \delta\phi^2/4) \cos \hat{\varphi} + \sqrt{\frac{1}{8}} \delta\phi^2 E_{\text{J}\Sigma} \cos \hat{\varphi} \cos(2\omega_d t) + \sqrt{2} E_{\text{J}\Sigma} \cos \hat{\varphi} \delta\phi \cos(\omega_d t). \quad (\text{C3})$$

Following Appendix A 2, we perform the generalized Schrieffer-Wolff transformation and obtain the following static effective Hamiltonian in the rotating frame

$$\begin{aligned} \hat{\mathcal{H}}_{\text{SQ}} = & \Delta \hat{a}^\dagger \hat{a} - \frac{\sqrt{2}E_{\text{J}\Sigma}\varphi_{\text{zps}}^4}{4} \left(1 - \frac{\delta\phi^2}{4}\right) \hat{a}^{\dagger 2} \hat{a}^2 - \frac{\sqrt{2}\delta\phi E_{\text{J}\Sigma}}{4} \left[\left(\varphi_{\text{zps}}^2 - \frac{\varphi_{\text{zps}}^4}{2}\right) (\hat{a}^{\dagger 2} + \hat{a}^2) \right. \\ & \left. - \frac{\varphi_{\text{zps}}^4}{3} (\hat{a}^\dagger \hat{a}^3 + \hat{a}^{\dagger 3} \hat{a}) \right] + \frac{\sqrt{2}\delta\phi^2 E_{\text{J}\Sigma}\varphi_{\text{zps}}^4}{192} (\hat{a}^{\dagger 4} + \hat{a}^4) + \frac{\delta\phi^2 E_{\text{J}\Sigma}\varphi_{\text{zps}}^4}{2\omega_d} \left[\left(-1 + \frac{\delta\phi^2}{12}\right) \hat{a}^\dagger \hat{a} + \frac{\delta\phi}{4} (\hat{a}^{\dagger 2} + \hat{a}^2) \right]. \quad (\text{C4}) \end{aligned}$$

Similarly, the static effective master equation is given by

$$\begin{aligned} \frac{\partial \hat{\rho}_{\text{S}}}{\partial t} = & -\frac{i}{\hbar} [\hat{\mathcal{H}}_{\text{SQ}}, \hat{\rho}_{\text{S}}] + \frac{4}{\hbar} \kappa(\omega_d/2) \left\{ n(\omega_d/2) \mathcal{D}\{\hat{a}\} \hat{\rho}_{\text{S}} + [1 + n(\omega_d/2)] \mathcal{D}\{\hat{a}^\dagger\} \hat{\rho}_{\text{S}} \right\} \\ & + \frac{1}{\hbar} \left(\frac{\sqrt{2}\delta\phi E_{\text{J}}^S \varphi_{\text{zps}}^2}{4\hbar\omega_d} \right)^2 \kappa(3\omega_d/2) \left\{ n(3\omega_d/2) \mathcal{D}\{3\hat{a}^\dagger + \delta\phi\hat{a}\} \hat{\rho}_{\text{S}} + [1 + n(3\omega_d/2)] \mathcal{D}\{3\hat{a} + \delta\phi\hat{a}^\dagger\} \hat{\rho}_{\text{S}} \right\} \\ & + \frac{1}{\hbar} \left(\frac{\delta\phi\sqrt{2}G_{2,S}}{3\hbar\omega_d} \right)^2 \kappa(5\omega_d/2) \left\{ n(5\omega_d/2) \mathcal{D}\{\hat{a}^\dagger\} \hat{\rho}_{\text{S}} + [1 + n(5\omega_d/2)] \mathcal{D}\{\hat{a}\} \hat{\rho}_{\text{S}} \right\}. \quad (\text{C5}) \end{aligned}$$

Appendix D: SNAIL and STS Kerr-cat qubit

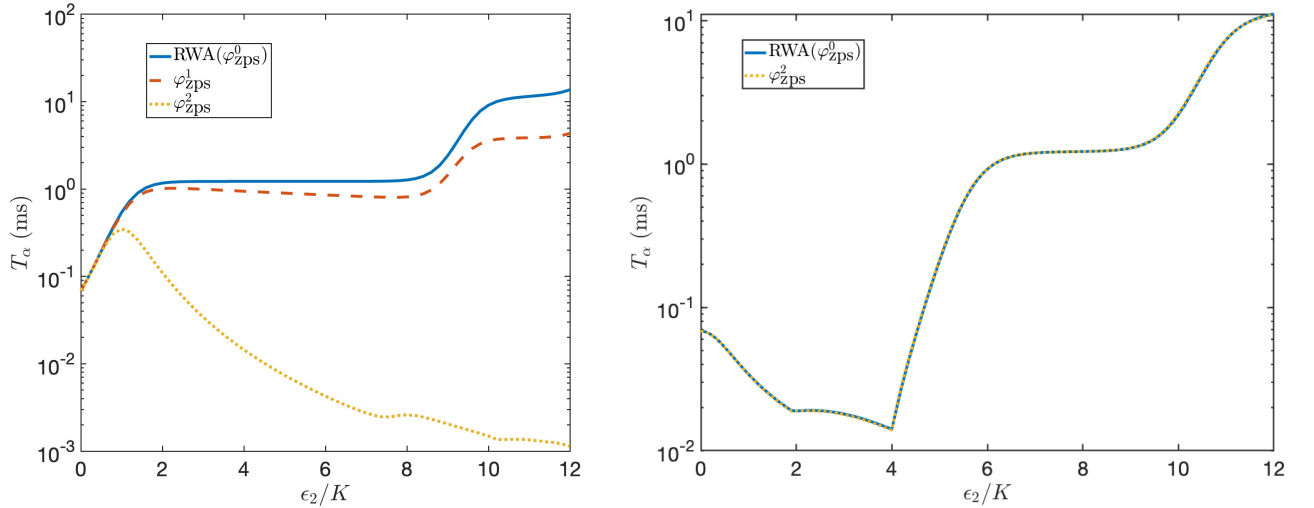


Figure 12. T_α of the Kerr-cat qubit as a function of the two-photon drive strength ϵ_2/K taking $K = 14.4\text{MHz}$ (a) for a SNAIL design and (b) for a STS design.

We compare the SNAIL and STS Kerr-cat qubit with realistic parameters from experiments. Using the quantum master equations calculated in Ref. [21], we plot T_α of a SNAIL Kerr-cat qubit in Fig. 12 (a) for a Kerr coefficient of 14.4 MHz, temperature of $T_{\omega_d/2} = 82.5\text{ mK}$, and decay rate of $\kappa(\omega_d/2)/h = 26\text{ kHz}$. All the other parameters were taken from Ref. [21]. Keeping the coupling and temperature of the environment the same as above, and fixing the parameters in STS to obtain $K/h = 14.4\text{ MHz}$, we plot T_α for the STS Kerr-cat qubit in Fig. 12(b). We take up to $\mathcal{O}(\varphi_{\text{zps}}^2)$ terms in both cases in the master equation. Unlike the case of STS where the system bath coupling at $\mathcal{O}(\varphi_{\text{zps}}^1)$ is a scalar and does not induce any dynamics, in the case of SNAIL it leads to a small reduction in lifetime (see the dashed orange curve in Fig. 12(a)). Further, the $\mathcal{O}(\varphi_{\text{zps}}^2)$ which leads to two-photon dissipative effects in the SNAILs leading to a strong reduction in lifetime (see the yellow dashed curve in Fig. 12(a)), has no effect in the lifetime in the case of STS. We observed in the Appendix B that the two photon heating and cooling effects enters the STS dynamics only at $\mathcal{O}(\varphi_{\text{zps}}^3)$ and is proportional to the asymmetry of the SQUID junctions. Hence, the two-photon dissipative effects can be mitigated by making the junctions as symmetric as possible. One features that leads to the reduction in T_α of the STS Kerr-cat qubit is the presence of the extra term Λ in the STS Kerr-cat Hamiltonian in Eq. (7) compared to the standard Kerr-cat Hamiltonian in Eq. (1) (leading to a dip in lifetime for $\epsilon_2/K \leq 4$ in

Fig. 12(b)). In inset of Fig. 4, we showed that the effect of Λ can be cancelled by adding a drive dependent detuning to the Kerr-cat Hamiltonian leading to the restoration of the staircase type lifetime plot.

-
- [1] Y. Nakamura, Y. A. Pashkin, and J. Tsai, Coherent control of macroscopic quantum states in a single-Cooper-pair box, *Nature* **398**, 786 (1999).
- [2] J. Koch, T. M. Yu, J. Gambetta, A. A. Houck, D. I. Schuster, J. Majer, A. Blais, M. H. Devoret, S. M. Girvin, and R. J. Schoelkopf, Charge-insensitive qubit design derived from the Cooper pair box, *Physical Review A* **76**, 042319 (2007).
- [3] V. E. Manucharyan, J. Koch, L. I. Glazman, and M. H. Devoret, Fluxonium: Single Cooper-pair circuit free of charge offsets, *Science* **326**, 113 (2009).
- [4] A. Grimm, N. E. Frattini, S. Puri, S. O. Mundhada, S. Touzard, M. Mirrahimi, S. M. Girvin, S. Shankar, and M. H. Devoret, Stabilization and operation of a Kerr-cat qubit, *Nature* **584**, 205 (2020).
- [5] L. B. Nguyen, Y. Kim, A. Hashim, N. Goss, B. Marinelli, B. Bhandari, D. Das, R. K. Naik, J. M. Kreikebaum, A. N. Jordan, *et al.*, Programmable Heisenberg interactions between floquet qubits, *Nature Physics* , 1 (2024).
- [6] S. M. Anton, C. Müller, J. S. Birenbaum, S. R. O’Kelley, A. D. Fefferman, D. S. Golubev, G. C. Hilton, H.-M. Cho, K. D. Irwin, F. C. Wellstood, G. Schön, A. Shnirman, and J. Clarke, Pure dephasing in flux qubits due to flux noise with spectral density scaling as $1/f^\alpha$, *Physical Review B* **85**, 224505 (2012).
- [7] G. Ithier, E. Collin, P. Joyez, P. J. Meeson, D. Vion, D. Esteve, F. Chiarello, A. Shnirman, Y. Makhlin, J. Schrieffer, and G. Schön, Decoherence in a superconducting quantum bit circuit, *Physical Review B* **72**, 134519 (2005).
- [8] L. B. Nguyen, Y.-H. Lin, A. Somoroff, R. Mencia, N. Grabon, and V. E. Manucharyan, High-coherence fluxonium qubit, *Physical Review X* **9**, 041041 (2019).
- [9] F. Yoshihara, K. Harrabi, A. O. Niskanen, Y. Nakamura, and J. S. Tsai, Decoherence of flux qubits due to $1/f$ flux noise, *Physical Review Letter* **97**, 167001 (2006).
- [10] S. Puri, S. Boutin, and A. Blais, Engineering the quantum states of light in a Kerr-nonlinear resonator by two-photon driving, *npj Quantum Information* **3**, 18 (2017).
- [11] H. Goto, Universal quantum computation with a nonlinear oscillator network, *Physical Review A* **93**, 050301 (2016).
- [12] S. Puri, A. Grimm, P. Campagne-Ibarcq, A. Eickbusch, K. Noh, G. Roberts, L. Jiang, M. Mirrahimi, M. H. Devoret, and S. M. Girvin, Stabilized cat in a driven nonlinear cavity: A fault-tolerant error syndrome detector, *Physical Review X* **9**, 041009 (2019).
- [13] N. E. Frattini, R. G. Cortiñas, J. Venkatraman, X. Xiao, Q. Su, C. U. Lei, B. J. Chapman, V. R. Joshi, S. Girvin, R. J. Schoelkopf, *et al.*, The squeezed Kerr oscillator: Spectral kissing and phase-flip robustness, [arXiv:2209.03934](https://arxiv.org/abs/2209.03934) (2022).
- [14] J. Venkatraman, R. G. Cortinas, N. E. Frattini, X. Xiao, and M. H. Devoret, A driven quantum superconducting circuit with multiple tunable degeneracies, [arXiv:2211.04605](https://arxiv.org/abs/2211.04605) (2023).
- [15] A. Hajr, B. Qing, K. Wang, G. Koolstra, Z. Pedramrazi, Z. Kang, L. Chen, L. B. Nguyen, C. Junger, N. Goss, I. Huang, B. Bhandari, N. E. Frattini, S. Puri, J. Dressel, A. N. Jordan, D. I. Santiago, and I. Siddiqi, High-coherence Kerr-cat qubit in 2D architecture, [arXiv:2404.16697](https://arxiv.org/abs/2404.16697) (2024).
- [16] D. Iyama, T. Kamiya, S. Fujii, H. Mukai, Y. Zhou, T. Nagase, A. Tomonaga, R. Wang, J.-J. Xue, S. Watabe, *et al.*, Observation and manipulation of quantum interference in a superconducting Kerr parametric oscillator, *Nature Communications* **15**, 86 (2024).
- [17] J. Chávez-Carlos, T. L. Lezama, R. G. Cortiñas, J. Venkatraman, M. H. Devoret, V. S. Batista, F. Pérez-Bernal, and L. F. Santos, Spectral kissing and its dynamical consequences in the squeeze-driven Kerr oscillator, *npj Quantum Information* **9**, 76 (2023).
- [18] R. Gautier, A. Sarlette, and M. Mirrahimi, Combined dissipative and Hamiltonian confinement of cat qubits, *PRX Quantum* **3**, 020339 (2022).
- [19] S. Kwon, S. Watabe, and J.-S. Tsai, Autonomous quantum error correction in a four-photon Kerr parametric oscillator, *npj Quantum Information* **8**, 40 (2022).
- [20] S. Puri, L. St-Jean, J. A. Gross, A. Grimm, N. E. Frattini, P. S. Iyer, A. Krishna, S. Touzard, L. Jiang, A. Blais, S. T. Flammia, and S. M. Girvin, Bias-preserving gates with stabilized cat qubits, *Science Advances* **6**, eaay5901 (2020).
- [21] J. Venkatraman, X. Xiao, R. G. Cortiñas, and M. H. Devoret, On the static effective Lindbladian of the squeezed Kerr oscillator, [arXiv:2209.11193](https://arxiv.org/abs/2209.11193) (2022).
- [22] X. You, J. A. Sauls, and J. Koch, Circuit quantization in the presence of time-dependent external flux, *Physical Review B* **99**, 174512 (2019).
- [23] D. Ruiz, R. Gautier, J. Guillaud, and M. Mirrahimi, Two-photon driven Kerr quantum oscillator with multiple spectral degeneracies, *Physical Review A* **107**, 042407 (2023).
- [24] C. K. Andersen, A. Kamal, N. A. Masluk, I. M. Pop, A. Blais, and M. H. Devoret, Quantum versus classical switching dynamics of driven dissipative Kerr resonators, *Physical Review Applied* **13**, 044017 (2020).
- [25] A. Miano, G. Liu, V. Sivak, N. Frattini, V. Joshi, W. Dai, L. Frunzio, and M. Devoret, Frequency-tunable Kerr-free three-wave mixing with a gradiometric snail, *Applied Physics Letters* **120** (2022).
- [26] A. S. Darmawan, B. J. Brown, A. L. Grimsmo, D. K. Tuckett, and S. Puri, Practical quantum error correction with the XZZX code and Kerr-cat qubits, *PRX Quantum* **2**, 030345 (2021).
- [27] X. He, Y. Lu, D. Bao, H. Xue, W. Jiang, Z. Wang, A. Roudsari, P. Delsing, J. Tsai, and Z. Lin, Fast generation of Schrödinger cat states using a Kerr-tunable superconducting resonator, *Nature communications* **14**, 6358 (2023).

- [28] M. Mirrahimi, Z. Leghtas, V. V. Albert, S. Touzard, R. J. Schoelkopf, L. Jiang, and M. H. Devoret, Dynamically protected cat-qubits: a new paradigm for universal quantum computation, *New Journal of Physics* **16**, 045014 (2014).
- [29] J. Venkatraman, *Controlling the effective Hamiltonian of a driven quantum superconducting circuit*, Ph.D. thesis, Yale University (2023).
- [30] P. Kapitza, Dynamic stability of the pendulum with vibrating suspension point (1951), *Collected papers of PL Kapitza* **2**, 714 (1965).
- [31] Z. Leghtas, S. Touzard, I. M. Pop, A. Kou, B. Vlastakis, A. Petrenko, K. M. Sliwa, A. Narla, S. Shankar, M. J. Hatridge, M. Reagor, L. Frunzio, R. J. Schoelkopf, M. Mirrahimi, and M. H. Devoret, Confining the state of light to a quantum manifold by engineered two-photon loss, *Science* **347**, 853 (2015).
- [32] R. Lescanne, M. Villiers, T. Peronin, A. Sarlette, M. Delbecq, B. Huard, T. Kontos, M. Mirrahimi, and Z. Leghtas, Exponential suppression of bit-flips in a qubit encoded in an oscillator, *Nature Physics* **16**, 509 (2020).
- [33] C. Berdou, A. Murani, U. Réglade, W. Smith, M. Villiers, J. Palomo, M. Rosticher, A. Denis, P. Morfin, M. Delbecq, T. Kontos, N. Pankratova, F. Rautschke, T. Peronin, L.-A. Sellem, P. Rouchon, A. Sarlette, M. Mirrahimi, P. Campagne-Ibarcq, S. Jezouin, R. Lescanne, and Z. Leghtas, One hundred second bit-flip time in a two-photon dissipative oscillator, *PRX Quantum* **4**, 020350 (2023).
- [34] U. Réglade, A. Bocquet, R. Gautier, A. Marquet, E. Albertinale, N. Pankratova, M. Hallén, F. Rautschke, L.-A. Sellem, P. Rouchon, *et al.*, Quantum control of a cat-qubit with bit-flip times exceeding ten seconds, [arXiv:2307.06617](https://arxiv.org/abs/2307.06617) (2023).
- [35] R. Gautier, M. Mirrahimi, and A. Sarlette, Designing high-fidelity zeno gates for dissipative cat qubits, *PRX Quantum* **4**, 040316 (2023).
- [36] J. Guillaud and M. Mirrahimi, Repetition cat qubits for fault-tolerant quantum computation, *Physical Review X* **9**, 041053 (2019).
- [37] H. Putterman, J. Iverson, Q. Xu, L. Jiang, O. Painter, F. G. S. L. Brandão, and K. Noh, Stabilizing a bosonic qubit using colored dissipation, *Physical Review Letter* **128**, 110502 (2022).
- [38] S. Touzard, A. Grimm, Z. Leghtas, S. O. Mundhada, P. Reinhold, C. Axline, M. Reagor, K. Chou, J. Blumoff, K. M. Sliwa, S. Shankar, L. Frunzio, R. J. Schoelkopf, M. Mirrahimi, and M. H. Devoret, Coherent oscillations inside a quantum manifold stabilized by dissipation, *Physical Review X* **8**, 021005 (2018).
- [39] T. Aoki, T. Kanao, H. Goto, S. Kawabata, and S. Masuda, Control of the zz coupling between Kerr cat qubits via transmon couplers, *Physical Review Applied* **21**, 014030 (2024).
- [40] Y.-H. Kang, Y. Xiao, Z.-C. Shi, Y. Wang, J.-Q. Yang, J. Song, and Y. Xia, Effective implementation of nonadiabatic geometric quantum gates of cat-state qubits using an auxiliary qutrit, *New Journal of Physics* **25**, 033029 (2023).
- [41] Y. Suzuki, S. Kawabata, T. Yamamoto, and S. Masuda, Quantum state tomography for Kerr parametric oscillators, *Physical Review Applied* **20**, 034031 (2023).
- [42] S. Boutin, D. M. Toyli, A. V. Venkatramani, A. W. Eddins, I. Siddiqi, and A. Blais, Effect of higher-order nonlinearities on amplification and squeezing in josephson parametric amplifiers, *Physical Review Applied* **8**, 054030 (2017).
- [43] N. E. Frattini, *Three-wave mixing in superconducting circuits: stabilizing cats with SNAILs*, Ph.D. thesis, Yale University (2021).
- [44] X. You, J. A. Sauls, and J. Koch, Circuit quantization in the presence of time-dependent external flux, *Physical Review B* **99**, 174512 (2019).
- [45] J. Venkatraman, X. Xiao, R. G. Cortiñas, A. Eickbusch, and M. H. Devoret, Static effective Hamiltonian of a rapidly driven nonlinear system, *Physical Review Letter* **129**, 100601 (2022).